Long-range transported continental aerosol in the Eastern North Atlantic: three multiday event regimes influence cloud condensation nuclei

Francesca Gallo[1*], Janek Uin[2], Kevin J. Sanchez[3], Richard H. Moore[3], Jian Wang[4], Robert Wood[5], Fan Mei[6], Connor Flynn[7], Stephen Springston[2], Eduardo B. Azevedo[8], Chongai Kuang[2], Allison C. Aiken[1]

[1]Earth and Environmental Sciences Division, Los Alamos National Laboratory, Los Alamos, NM, USA
[2]Environment and Climate Science Department, Brookhaven National Laboratory, Upton, NY, USA
[3]NASA Langley Research Centre, Hampton, VA
[4]Center for Aerosol Science and Engineering, Department of Energy, Environmental and Chemical Engineering, Washington University in St. Louis, St. Louis, MO, USA
[5]Department of Atmospheric Sciences, University of Washington, Seattle, USA
[6]Atmospheric Measurement and Data Sciences, Pacific Northwest National Laboratory, Richland, WA, USA
[7]School of Meteorology, University of Oklahoma, OK, USA
[8]Group of Climate, Meteorology and Global Change (CMMG), University of Azores, Portugal

*now at NASA Langley Research Centre, Hampton, VA

Correspondence to: Allison C. Aiken (aikenac@lanl.gov), Francesca Gallo (francesca.gallo@nasa.gov)

Abstract.

The Eastern North Atlantic (ENA) is a region dominated by pristine marine environment and subtropical marine boundary layer clouds. Under unperturbed atmospheric conditions, the regional aerosol regime at ENA varies seasonally due to different seasonal surface-ocean biogenic emissions, removal processes, and meteorological regimes. However, during periods when the marine boundary layer aerosol at ENA is impacted by particles transported from continental sources, aerosol properties within the marine boundary layer change significantly, affecting the concentration of cloud condensation nuclei (CCN). Here, we investigate the impact of long-range transported continental aerosol on the regional aerosol regime at ENA using data collected at the U.S. Department of Energy's (DOE) Atmospheric Radiation Measurement (ARM) User Facility on Graciosa Island in 2017 during the Aerosol and Cloud Experiments (ACE-ENA) campaign. We develop an algorithm that integrates number concentrations of particles with optical particle dry diameter (D_p) between 100 and 1000 nm, single scattering albedo, and black carbon concentration to identify multiday events (with duration > 24 consecutive hours) of long-range continental aerosol transport at ENA. In 2017, we detected nine multiday events of long-range transported particles that correspond to ~7.5% of the year. For each event, we perform HYSPLIT 10-day backward trajectories analysis, and we evaluate CALIPSO aerosol products to assess respectively origins and compositions of aerosol particles arriving at ENA. Subsequently, we group the events into three categories 1) mixture of dust and marine aerosols , 2) mixture of marine and polluted continental aerosols from industrialized areas, and 3) biomass burning aerosol from North America and Canada, and we evaluate their influence on aerosol population and cloud condensation nuclei in terms of potential activation fraction and concentrations at supersaturation of 0.1% and 0.2%. The arrival of plumes dominated by the mixture of dust and marine aerosol at ENA in the winter caused significant increases in baseline N_{tot}. Simultaneously, the baseline particle size modes and CCN potential activation fraction remained almost unvaried, while cloud condensation nuclei concentrations increased proportionally to N_{tot}. Events dominated by mixture of marine and polluted continental aerosols in spring, fall, and winter led to statistically significant increase in baseline N_{tot}, shift towards larger particular sizes, higher CCN potential activation fractions, and cloud condensation nuclei concentrations > 170% and up to 240% higher than during baseline regime. Finally, the transported aerosol plumes characterized by elevated concentration of biomass burning aerosol from continental wildfires detected in the summertime did not statistically contribute to increase baseline aerosol particle concentrations at ENA. However, particles diameters were

larger than under baseline conditions and CCN potential activation fractions was > 75% higher. Consequentially, cloud concentration nuclei concentrations increased ~115% during the period affected by the biomass burning events. Our results suggest that, through the year, multiday events of long-range continental aerosol transport periodically affect ENA and represent a significant source of CCN in the marine boundary layer. Based on our analysis, in 2017, the multiday aerosol plume transport dominated by mixture of dust and marine aerosol, mixture of marine and polluted continental aerosols, and biomass burning aerosols caused increases in N_{CCN} baseline regime of respectively 6.6%, 8%, and 7.4% at SS 0.1% (and respectively 6.5%, 8.2%, and 7.3% at SS 0.2%) at ENA.

1 Introduction

Atmospheric aerosols are one of the key components of the climate system interacting with clouds and affecting cloud radiative properties, height, and water content (Twomey, 1974; Albrecht, 1989). Remote marine low-lying cloud regions are thought to be the most affected by changes in aerosol properties because clouds are optically thin and the background aerosol concentration is low (Moore et al., 2013; Rosenfeld et al., 2014; Wood et al., 2015). However, the interactions among marine boundary layer (MBL) aerosol number concentration (N_{tot}), cloud condensation nuclei (CCN) and cloud droplet concentration under different aerosol loading are still poorly understood and remain one of the largest sources of uncertainties in climate models and future climate projections (Bony, 2005; Carslaw et al., 2013; Fan et al., 2016; Seinfeld et al., 2016).

Over the past years, an increased number of studies and field campaigns have been dedicated to remote marine low-clouds systems in the North Atlantic Ocean to improve the parametrization of aerosol and cloud processes in the MBL (Albrecht et al., 1995; Rémillard et al., 2012; Wood et al., 2015; Behrenfeld et al., 2019; Sorooshian et al., 2020; Redemann et al., 2021; Wang et al., 2021). The observations collected have provided invaluable insights into the potential role of aerosols in controlling cloud properties and precipitation. Namely, perturbations in aerosol properties have been found to be associated with strong synoptic meteorological variability (Rémillard et al., 2012), variations in CCN number concentrations (N_{CCN}) and cloud optical depth (Liu et al., 2016), and increases in larger longer lasting cloud cover, precipitation suppression, and cooling (Rosenfeld et al., 2014). Further efforts have been focused on examining the influence of long-range transport of continental particles on unperturbed aerosol marine regimes. These studies underline the potential of long-range transported aerosols of continental origins to alter the concentration of aerosols, cloud condensation nuclei, cloud droplets and efficiency of precipitation formation (Garrett and Hobbs, 1995; Dadashazar et al., 2021; Tomlin et al., 2021; Wang et al., 2021). Despite the importance of this topic, a quantitative understanding of the cloud condensation nuclei budget changes over the North Atlantic Ocean as a function of aerosol perturbations due to continental emissions is still missing and the aerosol indirect forcing remains uncertain (Carslaw et al., 2013).

With the goal of characterizing aerosol and cloud interactions in extratropical marine environments, in 2013, the U.S. Department of Energy's (DOE) Atmospheric Radiation Measurement (ARM) User Facility established a long-term fixed site Facility in the Eastern North Atlantic (ENA) (Mather and Voyles, 2013; Dong et al., 2014; Logan et al., 2014; Feingold and McComiskey, 2016), in the Azores Archipelago. The ENA ARM site is located on the remote Graciosa Island, one of the smallest and least populated islands of the archipelago. Variations in synoptic meteorological conditions and the entrainment of transported continental aerosol particles from the free troposphere into the marine boundary layer periodically affect the local conditions in the Archipelago throughout the year. These features make the ENA ARM site well-suited for collecting open ocean representative measurements, and an excellent location to investigate the impact of long-range transport of continental particles on low-cloud systems in pristine marine regions (Wood et al., 2015; Wang et al., 2021).

The ENA Facility includes an Aerosol Observing System (AOS) for the continuous measurements of aerosol physical, optical, and chemical properties, and the associated meteorological parameters at time resolutions from seconds to minutes (Uin et al., 2019). In situ AOS observations provide an unprecedented opportunity to robustly study the interaction between aerosols and

clouds to achieve a quantitative understanding of the key controlling processes that drive aerosol properties and the CCN budget in the MBL. In addition to the AOS routine measurements, during two Intensive Operating Periods (IOPs) (June-July 2017 and January-February 2018) of the ARM Aerosol and Cloud Experiments in the Eastern North Atlantic (ACE-ENA) field campaign, the ARM Aerial Facility (AAF) Gulfstream-159 (G-1) research aircraft flew over the ENA site and provided

5   in-situ characterizations of the marine boundary layer and lower free troposphere structure, as well as the vertical distribution and horizontal variability of low clouds and aerosols (Wang et al., 2021). High correlation (slope = 1.04 +/- 0.01, r^2 = 0.7) between AOS submicron number concentrations of particles at the ENA fixed site and AAF measurements were found during the summer indicating the broader regional representativeness of the AOS surface measurements when the boundary layer is well mixed (Gallo et al., 2020).

10   The recent results from the ACE-ENA campaigns have advanced the knowledge of aerosol process (Zawadowicz et al., 2020; Wang et al., 2021b; Zheng et al., 2021), and cloud structures and processes (Gao et al., 2020; Yeom et al., 2021) in the remote MBL, as well as have allowed the evaluation of algorithms for remote sensing retrievals (Wu et al., 2020). However, many mechanisms underlying aerosol-cloud interactions over the North Atlantic remain unresolved. Within the ACE-ENA scientific objectives yet to be addressed, the complete understanding of the key controlling processes that shape CCN budget in the MBL

15   is critical (Wang et al., 2021) Motivated by this need, in this study, we leverage the AOS datasets collected at ENA duringthe entire year 2017 to constrain the influence of long-range transported particles with different continental origins on the cloud condensation nuclei concentrations in the pristine marine environment. First, we develop an algorithm that integrates aerosol property indicators of the presence of continental particles to detect multiday (> 24 consecutive hours) transported aerosol plume events at ENA. Changes in specific aerosol properties caused by the arrival of continental air masses over the ENA

20   region have been described in previous literature. Namely, increased concentrations of submicron aerosol particles have been reported in the Western and Eastern North Atlantic by a number of previous studies (Garrett and Hobbs, 1995; Logan et al., 2014; Pennypacker and Wood, 2017; Sanchez et al., 2022). Simultaneously, elevated levels of black carbons (BC) and low submicron single scattering albedo (SSA) values in different locations in the North Atlantic region have been associated with the presence of continental air masses containing products from incomplete fossil fuel combustion and biomass burning

25   (Kleefeld, 2002; Junker et al., 2006; Costabile et al., 2013; O'Dowd et al., 2014; China et al., 2015; Cavalli et al., 2016). Based on these studies, we develop our algorithm and define specific thresholds for each of the aerosol parameters discussed above to detect periods affected by continental air masses (Section 2.2).

Once the multiday aerosol plume transport events have been detected by the algorithm, we assess aerosol regimes at ENA under both regional aerosol baseline conditions (Sect. 3.1) and during period of times impacted by the arrival of continental

30   aerosol particles (Sect. 3.2). Namely, we first evaluate aerosol sources and sinks under unperturbed marine conditions providing the necessary framework to understand the influence of continental transport on marine aerosol population and CCN budget. Subsequently, we determine the origins and types of aerosols transported at ENA during the multiday events using Hysplit backward trajectories and Cloud-Aerosol Lidar and Infrared Pathfinder Satellite Observations (CALIPSO) classification respectively, and we quantitatively assess the influence of the events on aerosol properties at ENA through

35   statistical analysis. In section 3.2 we present three case studies representatives of the diverse continental aerosol plumes arriving at ENA through the year: mixture of marine aerosols and dust (Sect. 3.2.1), mixture of polluted continental and marine aerosols (Sect. 3.2.2), and biomass burning aerosols (Sect. 3.2.3). In addition, we provide a summary statistic of multiday aerosol plume transport event influences on aerosol physical properties, such as variation in particle number concentrations and shifts in size distribution, and CCN potential activation factor and concentrations at ENA (Sect 3.2.4).

40   With this study, we aim to provide key observational constraints to parametrize the influence of changes in baseline N_{tot} and particle size modes due to aerosol perturbation events on CCN regimes. Ultimately, our results might be used as a proxy to estimate the CCN budget over remote oceans and to inform climate models improvements and validation.

2 Measurements and methodology

2.1 ENA ARM facility

Measurements of *in situ* aerosol properties examined in this study were collected though the Aerosol Observing System (AOS) at the ENA ARM fixed facility on Graciosa Island (39° 5' 28" N, 28° 1' 36" W) (Bullard et al., 2017; Uin et al., 2019; Uin and Smith, 2020), between January 1st, 2017 and December 31st, 2017. The ENA ARM AOS comprises of one container that samples aerosols using instrumentations connected to a central not-heated inlet located approximately 10 m above ground. A list of the AOS measurements analyzed here, including references for each instrument, is given in Table 1 and summarized in the following sections. Pressure for aerosol instruments is given at ambient conditions if not differently stated.

Prior to conducting any data analysis, periods impacted by local aerosol events (~23% of the 2017 datasets used in the study) were removed from submicron aerosol number concentration (N_{tot}), size distribution, single scattering albedo, black carbon, and cloud condensation nuclei datasets using the ENA-Aerosol Mask algorithm specifically developed for the AOS measurements at ENA (Gallo et al., 2020; Gallo and Aiken, 2022).

2.1.1 Aerosol physical properties

Measurement of submicron particle number concentrations (N_{tot}) with particle diameter (D_p) > 10 nm are made with a Condensation Particle Counter (CPC) Model 3772 (TSI, Inc., Shoreview, MN, USA) (Kuang et al., 2019). A Ultra-High Sensitivity Aerosol Spectrometer (UHSAS) (Droplet Measurement Technologies, Inc., Longmont, CO, USA) is used for sizing particles with D_p between 70 and 1000 nm (Uin, 2016a). Size distributions of submicron aerosol particles are described by separating the data into three size modes: 1) Aitken (At) mode aerosols with $D_p \leq 100$ nm, 2) Accumulation (Ac) mode aerosols with D_p between 100 and 300, and 3) Large Accumulation (LA) mode aerosol with D_p between 300 and 1000. The number concentration of the Accumulation (N_{Ac}) and Large Accumulation (N_{LA}) modes aerosol are directly measured by the UHSAS, while CPC and UHSAS measurements are combined to calculate the Aitken (N_{At}) mode as the difference between total particle number concentrations and the sum of the two larger modes: $N_{At} = N_{tot} - (N_{Ac} + N_{LA})$. Number concentrations of cloud condensation nuclei (N_{CCN}) are measured using a Cloud Condensation Nuclei (CCN) Counter (Droplet Measurements Technologies Inc.) at five levels of supersaturations from 0.1% to 1% (Roberts and Nenes, 2005; Rose et al., 2008; Uin, 2016b). Here, we utilize CCN measurements collected at the determined supersaturation (SS) levels of 0.1% and 0.2% which represent typical maximum supersaturations in marine boundary layer clouds where CCN activation occurs (Korolev and Mazin, 2003; Clarke and Kapustin, 2010; Wood, 2012). Furthermore, we combine CPC and CCN measurements to calculate the aerosol potential activation fraction (AF) as the ratio of N_{CCN} to the total submicron aerosol number. Finally, the hygroscopicity of aerosol particles with initial dry size from 50 to 250 nm is measured using a Humidified Tandem Differential Mobility Analyzer (HTDMA) (Brechtel Manufacturing, Inc.) (Uin, 2016c). Particle hygroscopic growth (HG) at subsaturated conditions is calculated as the ratio of the geometric mean mobility diameter of the humidified particles (d_m(RH)) (RH > 85%) to the dry diameter (d_d) (RH between 6.1% and 7.3%). According to the kappa-Köhler Theory (Petters and Kreidenweis, 2007) and using HG, we calculate the hygroscopicity parameter κ for dry particles with D_p = 50, 100, 150, 200, and 250 nm as:

$$\kappa = (HG^3 - 1) \left[\frac{\exp\left(\frac{A}{HG \, d_d}\right)}{RH} - 1 \right]$$

where A is the Kelvin parameter defined as:

$$A = \frac{4 \, \sigma_w \, M_w}{RT \, \rho_w}$$

M_w, σ_w and ρ_W are, respectively, the molar mass, the surface tension and the density of the water. R is the universal gas constant and T is the temperature. The instrument and its mode of operation are described in detail by (Lopez-Yglesias et al., 2014).

2.1.2 Aerosol optical and chemical properties

5   Aerosol absorption coefficients (B_{abs}) are measured at ENA using a three-wavelength Particle Soot Absorption Photometer (PSAP) at λ of 464, 529, and 648 nm. The instrument is described in detail by Bond et al. (1999) and Virkkula et al. (2005). The response of the PSAP is affected by mass flow calibration, filter loading, amount of light scattered by the particles, the flow rate, and the spot size of the sample (Bond et al., 1999; Virkkula et al., 2005; Virkkula, 2010). ARM archive PSAP data includes corrections for the mass flow calibration and filter loading (Springston, 2018). Aerosol scattering coefficients (B_{sca})

10   at ENA are measured at λ of 450, 550, and 700 nm using a TSI Integrating Nephelometer (TSI, model 3563) (Uin, 2016d). ARM archive Nephelometer data includes corrections for truncation and illumination errors (Uin, 2016d). Prior to measurement, the PSAP and nephelometer sample air passes through an impactor that periodically switches between 1 and 10 µm cut-point sizes (Uin et al., 2019). B_{abs} and B_{sca} values discussed in this study refer to measruements collcted at 1 µm cut-point sizes. The B_{sca} at 450 nm was scaled to the measured B_{abs} λ of 464 through interpolation based on Scattering Angstrom

15   Exponent (SAE) (Costabile et al., 2013). In this study we use aerosol light absorption (B_{abs}) and scattering (B_{sca}) coefficients to calculate the single scattering albedo (SSA) at 464 nm defined as SSA = (B_{sca}) / (B_{abs} + B_{sca}). Equivalent black carbon (BC) concentrations are estimated from (B_{abs}) with an assumed mass absorbing cross section of 6.4 m^2 g^{-1} at 648 nm (Bond and Bergstrom, 2006). Bulk particle composition measurements of the mass concentrations of non-refractory sulfate and organics are provided by an Aerodyne Research aerosol chemical speciation monitor (ACSM) (Ng et al., 2011; Watson, 2017).

20   ### 2.2 Multiday transported aerosol plume event identification algorithm and statistical analysis

We develop an algorithm to detect multiday transported aerosol plume events, which relies on the variations of physical and optical aerosol properties caused by long-range transport of particles in the Eastern North Atlantic. The application of the algorithm requires continuous measurements of the following three parameters: number concentrations of particles with optical particle dry diameter (D_p) between 100 and 1000 nm, submicron SSA at 464 nm wavelength, and black carbon concentration.

25   The measurements are averaged over 6-hour periods which are sufficiently short to detect variations in mass properties but also sufficiently long to remove the effect of hourly variations due to diurnal cycles and process that occur on small timescale (Wood et al., 2017; Dadashazar et al., 2021) and match the time frequency of the Hysplit backward trajectories discussed below (the utilization of 7- and 8-hour periods was also tested and lead to the same results). The thresholds for the three aerosol parameters are established based on earlier works conducted in the Eastern North Atlantic region that describe their variations

30   during the period affected by transport of continental air masses. Namely, Pennypacker and Wood (2017) observed at ENA daily median number concentrations of D_p 100 to 1000 nm particles above 100 cm^{-3} during periods dominated by high sea-level pressure and large-scale subsistence with air masses originating from North America approaching the Azores from the northwest. In the same study, the high median concentration of particles D_p 100-1000 nm regime was found to be associated with median and 75th percentile SSA values of 0.92 and 0.95 respectively, at 470 nm wavelength. Black carbon concentrations

35   ranging between 10 and 40 ng m^{-3} during clean conditions have been reported by field studies conducted in different locations in the North Atlantic (O'Dowd et al., 2004; Shank et al., 2012;; Cavalli et al., 2016). Quinn et al. (2019) and Sakerin et al. (2021) have reported average BC concentrations between 15 and 25 ng m^{-3} and 37 and 44 ng m^{-3} respectively in the Western North Atlantic during the NAAMES field campaigns and during cruise expeditions conducted between 2007 and 2020 over North Atlantic ocean. A threshold of 75 ng m^{-3} has been typically utilized to indicate the presence of continental influenced air

40   masses (Cooke et al., 1997; Kleefeld, 2002; Junker et al., 2006), while Pohl et al. 2014 have been used BC concentrations ranging from 20 and 44 ng m^{-3} to identify clean background in the subtropical Atlantic. In more recent works, Facchini et al.

(2008) and O'Dowd et al. (2014), determined BC 50 ng m^{-3} as a threshold value to identify combustion influences at Mace Head. Similarly, Saliba et al. (2020) and Lawler et al. (2020) used the same criterion to separate ambient marine from continental periods in the Western North Atlantic. Based on this literature, the algorithm flags the data as affected by long-range transported aerosols when the following conditions occur at the same time for at least 24 consecutive hours (four consecutive 6-hours periods): 1) median number concentration of D_p 100 - 1000 nm particles > 100 cm^{-3} over 6 hours period, 2) median submicron single scattering albedo at λ 464 nm < 0.95, and 3) mean black carbon concentrations > 40 ng m^{-3}. It is important noting that the utilization of medians instead of means for number concentration of D_p 100 - 1000 nm particles and SSA to constrain periods impacted by long-range transport events in Pennypacker and Wood (2017) is due to the need of minimize the potential impacts of unidentified outlier. In our study, we performed post data processing methods prior conducting any data analysis to removed short-duration high concentration aerosol events (Gallo et al., 2020) and we obtained similar mean and median values (difference between mean and median values < 12%) for the three parameters used to develop the multiday transported aerosol plume event identification algorithm. Therefore, to allow a better comparison of our results to the previous literatures the algorithm relies on the utilization of median values for number concentrations of particles with D_p between 100 and 1000 nm and submicron SSA at at 464 nm wavelength, and mean values for the black carbon concentration.

Once the multiday transported aerosol plumes events are detected, their origins and transport paths are evaluated by performing 10-day backward trajectories arriving at 50 m and 500 m above the ENA site. The analysis are conducted using the Hybrid Single-Particle Lagrangian Integrated Trajectory (HYSPLIT) 4 model (Stein et al., 2015) with a time step of 6 hours using National Center Environmental Prediction (NCEP) Global Data Assimilation System (GDAS) meteorological data and model vertical velocity as input. In addition, Cloud-Aerosol Lidar and Infrared Pathfinder Satellite Observations (CALIPSO) aerosol products within the first 1500 m of the vertical column (corresponding to the mean MBL depth over mid-latitude ocean (Rémillard et al., 2012)) are used, when available, to assess the predominant types of aerosol particles arriving at ENA during the events (Omar et al., 2009). CALIPSO classification includes six types of aerosol mixtures: clean continental, clean marine, dust, polluted continental, polluted dust, and smoke (Burton et al., 2013). Finally, to assess the correlation between origin and composition of the multiday transport events and their influence on baseline aerosol properties at ENA, we perform post hoc Tukey-Kramer Honest Significant Different (HSD) test (Haynes, 2013) determining whether the arrival of the continental aerosol plumes produced statistically significant changes onbaseline a) baseline aerosol number concentrations (ΔN_{tot}), b) aerosol mode sizes in terms of relative Aitken and Accumulation modes contributions to N_{tot} (expressed as the ratio between N_{At} and N_{Ac} (ΔN_{At} / N_{Ac}), and c) CCN potential activation fraction (ΔAF). The significance probability was assessed at the probability level of $p < 0.05$ and statistical analyses were performed using Igor Pro 8 with Statistic package (WaveMetrics Inc.).

3 Results and discussion

The entrainment of continental particles from long-range transport represents a significant source of aerosols over mid-latitude oceans and have the potential of altering the regional aerosol regimes (Garrett and Hobbs, 1995; Honrath, 2004; Roberts et al., 2006; García et al., 2017; Zhang et al., 2017; Zheng et al., 2018). Here, we apply the algorithm to detect multiday transported aerosol events at ENA during the year 2017. Measurements affected by local aerosol events were removed prior the application of the algorithm following Gallo et al. (2020). Once the events have been identified, we removed the measurements affected by the arrival of continental aerosol plumes and we extract the aerosol baseline conditions (period of times not affected by local aerosol events and/or long-range transported plumes) to assess the aerosol seasonal regimes at ENA (Section 3.1). Subsequently, the multiday aerosol plume transport events are examined and categorized based on origin and composition and

their impacts on aerosol physical properties, such as variation in particle number concentrations and shifts in size distribution, which affects the ability of particles to act as CCN are evaluated (Section 3.2).

3.1 Regional aerosol regime under baseline conditions

3.1.1 Concentration and size distribution of submicron aerosol particles

The concentration of submicron aerosol particles and their size distribution under baseline conditions at ENA show seasonal variations likely related to a combination of different regional emission sources and sink mechanisms. In remote marine regions like ENA, particles of marine origin, including sea spray aerosols and marine aerosols formed by biogenic volatile organic compounds produced by marine phytoplankton, dominate the aerosol population in the marine boundary layer (Rinaldi et al., 2010; Lapina et al., 2011; Sanchez et al., 2018). Overall, we found lower concentrations of submicron particles in the winter (Jan. – Feb., and Nov. -Dec. 2017) and higher during late spring and summer (Fig. 1). Namely, the minimum monthly N_{tot} mean value was observed in January 2017 (260 ± 143 cm^{-3}), while the maximum monthly N_{tot} mean value was reached in June 2017 (523 ± 259 cm^{-3}), approximately two times the winter minimum. Our results are consistent with earlier studies and field campaigns conducted in the North Atlantic ocean region which report low wintertime N_{tot} as the result of reduced contribution from ocean biological activities and higher occurrence of in-cloud precipitation and coalescence scavenging during winter months compared to the spring and summer (Pennypacker and Wood, 2017b; Zheng et al., 2018; Quinn et al., 2019; Gallo et al., 2022). Likewise, the concentration of particles in the Aitken and Accumulation modes follow similar seasonal trends with monthly mean minima in N_{At} and N_{Ac} in January 2017 ($N_{At} = 148\pm 81$ cm^{-3}) and in November ($N_{Ac} = 90 \pm 53$ cm^{-3}) respectively, and maxima in June 2017 ($N_{At} = 360 \pm 97$ cm^{-3} $N_{Ac} = 195 \pm 79$ cm^{-3}) (Fig. 1). Interestingly, we observed that summer (June – September 2017) mean N_{Ac} values, which are approximately doubled than in the winter, are considerably higher than the correspondent median N_{Ac} values (Fig. 1). There is minimal influence of local aerosol sources on Accumulation mode aerosols measurements at ENA and the data utilized here has been filtered to remove impact of potential local emissions (Gallo et al., 2020). However, in the summer, MBL baseline aerosol concentrations might be influenced by the entrainment of diluted and aged continental particles from the free troposphere which likely contributes to enhanced concentration of particles in the Accumulation mode (Wang et al., 2021a). This observation is consistent with previous studies investigating aerosol vertical profiles during the summer ACE-ENA field campaign (Wang et al., 2021b), and over the Western North Atlantic during the NASA North Atlantic Aerosol and Marine Ecosystems Study campaign (NAAMES). Particles in the Large Accumulation mode (not shown) showed the opposite seasonal trend reaching the maximum monthly mean value in the winter ($N_{LA} = 14 \pm 9$ cm^{-3} in January) and the lowest concentrations in the summer ($N_{LA} = 7\pm 4$ cm^{-3} in August). However, throughout the entire year, the total aerosol number concentration among the three particle modes is dominated by the Aitken mode (yearly mean Aitken mode contribution to $N_{tot} = 61\% \pm 3\%$) while the Accumulation mode is lower (yearly mean Accumulation mode contribution to $N_{tot} = 35\% \pm 4\%$) and Large Accumulation mode represents only a small percentage of N_{tot} (yearly mean Large Accumulation mode contribution to $N_{tot} = 3\% \pm 1\%$). Further analysis of the measured size distribution from the UHSAS instrument (measurement size range 70 - 1000 nm) during winter (January, February, November, and December 2017) and summer (May to September 2017) at ENA provide an insight into seasonal variations of particle size. In the wintertime mean particle size D_p peaks at 128 nm (Fig. 2a), while in the summer mean mode D_p is shifts towards slightly larger sizes peaking at 147 nm (Fig. 2b). While the UHSAS lower size limit is at $D_p = 70$ nm, the UHSAS size distribution measurements associated with the calculated N_{At}, and N_{Ac} and N_{La} suggest aerosol bimodal structure for both winter and summer. In the absence of the entrainment of particles of continental origins, the size distribution of particles in the MBL is shaped by different seasonal surface-ocean biogenic emissions, aerosol removal processes, and meteorological regimes (Behrenfeld et al., 2019). New particle formation events in the upper part of the decoupled MBL has been reported by previous studies and are due to a

combination of reduced existing aerosol surface area, passage of cold fronts, reactive gas availability and high actinic fluxes (Bates et al., 1998; Kolstad et al., 2009; Zheng et al., 2021). In the winter, more frequent precipitation, and drizzle at ENAlead to the removal of large particles, such as sea spray aerosols, and consequently low existing aerosol surface availability, which associated with wintertime cold temperature enhance the occurrence of new particles formation events. Once formed, the new particles grow into larger particles strongly contributing to N_{At}. The removal of Aitken mode particles is largely driven by coagulation, while the condensational growth into Ac mode is weak due to low DMS concentrations in the MBL and only represent a minor source of MBL N_{Ac} (Zheng et al., 2018). On the contrary, sea spray aerosol production at the surface ocean due to enhanced winter-time wind speeds up to 21.7 m s^{-1} (Aiken et al., 2019) substantially contributes to Large Accumulation modes concentrations explaining the higher N_{La} observed in January (Vignati et al., 2010; Zheng et al., 2018; Quinn et al., 2019). During late spring and summer, the phytoplankton bloom is responsible for strong ocean emissions of dimethylsulfide, whose oxidation products have been found to enhance the condensational growth of nucleation mode particles into the Aitken and subsequently to the Ac modes (O'Dowd et al., 1997; Andreae et al., 2003; Zheng et al., 2018). Furthermore, photochemistry and/or oxidation of oxygenated gas-phase organic compounds of marine origin produce secondary organic aerosols at the surface layer which contribute to the growth of Aitken mode particles during late summer when phytoplankton activity is lower (Mungall et al., 2017). In a previous study conducted at ENA between 2015 and 2018, Zheng et al. 2018 assessed the correlations between wind speeds and particle size. In the summer, no correlations between wind speeds and N_{At}, and N_{Ac} were reported while N_{LA} was observed to strongly correlate with wind speeds, therefore suggesting that the contribution from sea spray is limited to the Large Accumulation mode.

3.1.2 CCN concentrations and potential activation fraction

The concentration of CCN in the remote marine boundary layer is dominated by ocean-derived particles. Previous studies have reported that the major sources of CCN over the Atlantic Ocean include sea salt aerosols enriched in organics and marine biogenic gases that oxidize and condense onto existing particles (Charlson et al., 1987; Pandis et al., 1994; O'Dowd et al., 2004; Yoon et al., 2007; Korhonen et al., 2008; Quinn and Bates, 2011; Sanchez et al., 2018; Zheng et al., 2018). Here, we assess the seasonal variations of CCN concentrations (N_{CCN}) at ENA under baseline conditions, and we investigate the CCN potential activation fractions to evaluate how the different aerosol seasonal regimes affect the ability of the particles to act as CCN.

Throughout the year 2017, mean monthly CCN concentration values were low, as expected for clean marine environments (Ovadnevaite et al., 2014) and seasonal variations are noticeable at both super-saturations (Fig. 3). Lower monthly mean N_{CCN} values were reported in the winter and spring (minimum in December 2017 and $N_{CCN,0.1\%} = 69 \pm 27$ cm^{-3} at SS of 0.1 and $N_{CCN,0.2\%} = 108 \pm 38$ cm^{-3} cm^{-3} at SS 0.2%) while monthly N_{CCN} mean values were higher in the summer (maximum monthly N_{CCN} mean values in July 2017 and $= 141 \pm 53$ cm^{-3} at SS of 0.1 and $= 178 \pm 68$ cm^{-3} at SS 0.2%). The CCN potential activation fraction follows a different seasonal trend exhibiting higher values in late summer/fall and winter (mean AF SS 0.1% = 0.27 $\pm$ 0.03, and mean AF SS 0.1% = 0.41 $\pm$ 0.02) and lower in the spring (mean AF SS 0.1% = 0.22 $\pm$ 0.01, and mean AF SS 0.2% = 0.32 $\pm$ 0.04). The low number particle concentration and consequently low concentrations of cloud condensation nuclei observed in the MBL can be to a large degree attributable to reduced ocean biological activity in the winter. Furthermore, CCN removal through in-cloud coalescence scavenging processes associated with high occurrence of precipitation events in the winter and spring might also play a role in constraining CCN concentrations (Sharon et al., 2006; Zheng et al., 2018; Sanchez et al., 2022). However, the higher CCN potential activation fraction in wintertime than in the spring indicates that winter aerosol particles have a more elevated ability to act as cloud condensation nuclei. Supporting our finding, Wang et al. (2021a) reported high precipitation rate and increase CCN coalescence scavenging, accompanied by enhanced N_{Ac} activation at ENA during the ACE-ENA winter field campaign. A slightly lower ratio of N_{Ac} to N_{tot} in the winter than in the summer (mean Accumulation mode ratio to N_{tot} = 31% and 37% respectively in the winter and in the summer) suggest that particle

compositions play an important role in CCN formation at ENA. Consistent with our observations, earlier studies have pointed out that wind-generated sea spray aerosols enriched by particulate organic matter and biogenic sulfate, as observed at ENA in the winter are a stronger source of CCN than aerosols generated by phytoplankton activities at the surface ocean. (Quinn and Bates, 2011; Sanchez et al., 2018; O'Dowd et al., 2004). The higher summertime N_{CCN} observed here are in agreement with previous studies conducted at ENA which also found a correlation between elevated N_{CCN} and concentration of cloud droplet (Wood et al., 2015; Wang et al., 2021a) and reduced precipitation (Rémillard and Tselioudis, 2015; Giangrande et al., 2019), thus suggesting minimal CCN removal through wet scavenging. Simultaneously, strong VOC emissions at the surface ocean due to the final phase of the phytoplankton bloom and microbial activities leads to the formation of highly hygroscopic secondary sulfate particles which grow quickly into CCN by condensation and well explain the elevated N_{CCN} and potential activation fractions found here (Saliba et al., 2020; Zawadowicz et al., 2020).

3.2 Multiday transported aerosol plume events at ENA in 2017

We apply the algorithm for detecting multiday aerosol plume transport events at ENA to the in-situ aerosol measurements collected at ENA ARM during 2017. We identify 9 events affecting ENA through the entire year. The duration of the events was typically greater than 2 days with an average time period of 3 days, and total duration of 642 hours corresponding to ~7.5% of the year. A summary of the events, including duration, origins, aerosol CALIPSO classification and values of the three aerosol properties used to identify the events (median number concentration of D_p 100-1000 nm particles, mean single scattering albedo of submicron particles at λ 464 nm, and mean black carbon concentration) is shown in Table 2.

The origin of the air masses arriving at ENA and their paths, assessed by performing 10-day Hysplit backward trajectories, indicate a seasonal pattern likely controlled by seasonal meteorological regimes and atmospheric circulation in the Northern Hemisphere (Zhao et al., 2012). A number of studies reported Sahara dust intrusions into the North Atlantic MBL in the late fall and winter associated with cyclonic dust-storms in the North Africa region (Nakamae and Shiotani, 2013; Choobari et al., 2014; Laken et al., 2014; Logan et al., 2014; Cuevas et al., 2017). Similarly, air masses from Arctic might also represent a source of mineral dust at ENA in the spring (Zheng et al., 2018). In the case of the Arctic, the atmospheric load of dust particles is the result bare soil surface and glacial outwash plains and it is projected to increase over the next years as consequence of the retreat of glaciers (Bullard et al., 2016; Tobo et al., 2019). In accordance with these observations, we found two events of southward transport from northern African and Portuguese flows to ENA in the months of November and December 2017, likely favoured by Arctic anticyclone, polar vortex, and midlatitude circulation, and an event of transport from Arctic in March 2017. A large fraction of air masses arriving at ENA throughout the year are attributed to transport from industrialized continental areas as North Europe, Canada, and North America due to midlatitudes cyclones and convection (García et al., 2017). Continental aerosol particles are emitted in the boundary layer by anthropogenic processes and are subsequently transported for several days within the free troposphere before entrainment into the marine boundary layer over the North Atlantic ocean (Honrath, 2004; Wood et al., 2015; Cavalli et al., 2016). Here, we observed two aerosol transport events with Northern European origins in the months of January and April 2017. We also identified aerosol transports events from North America and Canada between May and September 2017. Our results are consistent with previous studies conducted in the North Atlantic region which reported dominant eastward direction from North America in the late spring and summers (Zhao et al., 2012) and high aerosol loading due to pollution outflow and biomass burning emissions (Honrath et al., 2004; Alves et al., 2007; Dzepina et al., 2015; García et al., 2017; Zheng et al., 2020; Wang et al., 2021b).

Analysis of CALIPSO aerosol products provide further insights on the type of aerosols transported. Consistent with the origin of the emission sources we observe dust and marine aerosol mixtures associated with transport from the Arctic and Canada in March 2017, and from North Africa in November and December 2017, while the airflows originating from industrialized areas (January, April, May, and October 2017) typically consisted of a mixture of polluted continental aerosol, smoke, and marine particles. Simultaneously, NASA Worldview VIRS 375 observations of the multiday aerosol plume transport events occurring

in August and September 2017 show elevated concentration of smoke over ENA due to a particularly intense wildfire season in North America and Canada, and therefore suggesting the presence of biomass burning aerosols as also previously observed by Zheng et al., 2020.

Finally, through the statistical analysis we were able to correlate aerosol plumes origin, composition, and the influences that they exert on N_{tot} and particle size seasonal regime at ENA to group the multiday transport events with similar characteristics into the following three categories: 1) Dust and marine mixture events - including March 2017 event with Arctic and Canada origins, and November and December 2017 events from North Africa, which caused statistically significant increase in baseline N_{tot} and statistically non-significant shifts in baseline size distribution and CCN potential activation fraction; 2) Polluted continental and marine mixture - including January, April, May, and October 2017 events originated in continental industrialized areas, which caused statistically significant changes in baseline submicron particle number concentration, baseline size distribution, and baseline CCN potential activation fraction, 3) Biomass burning - including August and September 2017 events, which caused statistically non-significant changes in baseline submicron aerosol particles, but did produce statistically significant shifts in baseline particle size distribution and an increase in the CCN potential activation fraction.

In the following three sections, we discuss case studies representatives of the diverse continental plumes arriving at ENA through the year, while in section 3.2.4, Table 3, and Fig. 8, we provide a summary statistic of the three multiday event regimes mentioned above.

3.2.1 Multiday transport event of dust and marine mixture aerosols from North Africa

The transport of air masses from North Africa to the North Atlantic ocean region during the winter is the result of the shift of the subtropical high pressure system south-eastward, and enhancing trade winds over the Sahara (Chiapello, 2005; Riemer et al., 2006; Alonso-Perez et al., 2011; Nakamae and Shiotani, 2013). Sahara dust intrusions in North Atlantic MBL have been reported by a number of studies (Choobari et al., 2014; Laken et al., 2014; Cuevas et al., 2017) especially between January and March (Alonso-Pérez et al., 2007). During the transport over the ocean, dust particles typically mix with marine aerosols (Peshev et al., 2019) undergoing heterogenous chemical reactions and removal mechanisms that alter their composition and size and as a consequence their influence on the CCN aerosol baseline regime. In this study, we identified the arrival of air masses from Western Sahara and Mauritania to ENA between December 7th and December 12th, 2017 (Fig. 4). Here, we assess CALIPSO retrievals, aerosol hygroscopicity parameters as a function of dry particle size (κ_{HTDMA}), non-refractory sulfate and organic mass, and concentrations of black carbon, and CO to confirm the nature of the aerosol particles arriving at ENA during the event (Fig. 7c). CALIPSO aerosol profiles indicate the presence of a mixture of dust and marine aerosol in the marine boundary layer. Simultaneously, κ_{HTDMA} values were = 0.22, 0.30, 0.37, 0.32, 0.37 respectively for dry particles with D_p = 50, 100, 150, 200, and 250 nm (Fig. 7a). For representative atmospheric aerosol particles, the hygroscopicity parameter κ_{HTDMA} ranges from 0 to 1.4 where high values (> 0.5) indicate very hygroscopic inorganic species such as sodium chloride, and low values indicate non-hygroscopic organic enriched compounds ($0.01 < \kappa_{HTDMA} < 0.5$ slightly to very hygroscopic, and $\kappa_{HTDMA} < 0.01$ non-hygroscopic components) (Petters and Kreidenweis, 2007). Although fresh emitted Sahara dust particles are typically not soluble, depending on the transport path and environmental conditions during the transport, heterogenous chemical interactions with other atmospheric particles and trace gases can influence their composition and enhance their hygroscopicity (Levin, 2005; Kallos et al., 2007; Astitha et al., 2010). The κ_{HTDMA} values observed here were accompanied by mean sulfate and organic mass concentrations respectively 1.63 µg m^{-3} and 0.91 µg m^{-3}, corresponding to 7-fold and 2-fold increase respectively in sulfate and organic masses compared to the baseline regime during the month of December 2017, suggesting that sulfate of marine and anthropogenic origins likely coat the dust making the particles more hygroscopic (Fig. 7c) (Koehler et al., 2009; Choobari et al., 2014; Zhang et al., 2014). Mean black carbon concentrations during the event were also higher than for the rest of the month (event mean BC = 101 ± 17 ng m^{-3} and up to 120 ng m^{-3} against baseline mean BC in December

2017 = 26 ± 8 ng m^{-3}), while CO levels remain constant (event mean CO = 101.4 ± 3 ppmv against baseline mean CO in December 2017 = 100.9 ± 9 ppmv). Consistent with our results, previous studies found that aerosol from biomass burning activities occurring during the dry season in the Sahel region (Boreal winter) can mix with the dust affecting the composition of the particles without transport of smoke over the Atlantic (Ben-Ami et al., 2009; Redemann et al., 2021). The arrival of the

5 aerosol plume at ENA was associated with an increase in mean submicron aerosol number concentration approximately doubled that under than under baseline conditions (mean event N_{tot} = 683 ± 135 cm^{-3} compared to monthly mean N_{tot} December 2017 = 313 ± 128 cm^{-3}). Aitken and Accumulation mode particle concentrations both double, while the relative contributions of the two modes to N_{tot} remained similar to baseline with mean Aitken contribution = 59% and mean Accumulation contribution = 38% of N_{tot} (N_{At} / N_{Ac} change = 0.3%) (Fig. 7b), indicating that the particles arriving at ENA during the event

10 had a size distribution similar to that of the regional aerosol. The peak of the size distribution in the Accumulation mode was at 127 nm for both event and baseline aerosol regimes, while the concentration of D_p > 200 nm particles was only 11% of N_{Ac}. Our results are in good agreement with previous studies conducted over the Central Atlantic ocean (Astitha et al., 2010) and in the Cape Verde region (Formenti et al., 2003) which found high number concentration of particles in the Aitken mode associated with the arrival of a mixture of dust and anthropogenic sulfate from North Africa. Namely, Formenti et al. (2003)

15 reported N_{At}/N_{Ac} ratio ~ 1.5-3 and size distribution dominated by particles with D_p 150 nm. The size of dust particles over the Atlantic ocean is the result of a combination of different source regions, dust generation mechanisms, atmospheric synoptic conditions and sink mechanisms. A number of previous study have been focused on the evolution of the size distribution of dusty aerosols during transport over the North Atlantic has been the focus of previous studies that reporting rapid loss of coarse mode particles due to gravitational settling and wet deposition just off the coast of Africa, while finer particles remain in

20 suspension and can be transported for longer distances (Maring, 2003; Kalashnikova and Kahn, 2008; Lawrence and Neff, 2009; Mahowald et al., 2014; Friese et al., 2016). The concentration of CCN increased during the event following a similar trend of N_{tot} (mean event N_{CCN} = 70 ± 27 cm^{-3} and 109 ± 31 cm^{-3} compared to monthly mean N_{CCN} December 2017 = 165 ± 32 cm^{-3}and 280 ± 36 cm^{-3} respectively for SS 0.1% and 0.2%, and corresponding increases by factors of 2.3 and 2.5 respectively over baseline value observed during the month of December 2017) leading to almost no change in CCN potential activation

25 fraction (event AF = 0.25 and 0.42 compared to AF in December 2017 = 0.26 and 0.42 respectively for SS 0.1% and 0.2%). Furthermore, the linear regression between N_{tot} and N_{CCN} during the event and under baseline conditions show similar slopes (at SS 0.1%: N_{CCN} = 0.23N_{tot}, and N_{CCN} = 0.18N_{tot} respectively during the event and under baseline conditions at SS 0.2%: N_{CCN} = 0.40N_{tot} and N_{CCN} = 0.30N_{tot} during the event and under baseline conditions respectively), indicating that the enhanced concentration of CCN observed during the event, is mainly due to higher N_{tot} (Fig. 7ed). Furthermore, when comparing the

30 potential activation fraction to the ratio of N_{Ac} and N_{At} we observed a good linear regression (AF= 0.42N_{Ac}/N_{At}, with r^2 =0.93 at SS 0.1%, and AF= 0.67N_{Ac}/N_{At}, with r^2 =0.90 at SS 0.2%) suggesting a strong correlation between CCN activated and particle size (Fig. 7e).

3.2.2 Multiday transport event of polluted continental and marine mixture aerosols from North Europe

35 Air masses from the Arctic and Europe occasionally reach the North East Atlantic during the spring months (Zheng et al., 2018), while transport from this region during summer and winter is rare (Zhang et al., 2017). Here, we describe a transport event of marine and polluted continental aerosol mixture at ENA which occurred between April 20th and April 22nd, 2017. The aerosol plume originated from the Arctic and before entraining into the MBL at ENA, travelled for several days over Northern Europe (Fig. 5). CALIPSO aerosol retrievals indicate the presence of a mixture of marine and polluted continental aerosols

40 (Table 2). Typically, during the transport to ENA, air masses are contaminated by industrial and urban pollution over industrialized European regions. The source apportionment of aerosol in Europe have been examined in previous studies by meaning of long-term studies and long-term station and satellite retrievals (Ng et al., 2010; Yang et al., 2020; Bressi et al.,

2021; Chen et al., 2022). Over Europe, the major contribution to aerosol emissions in Central and Northern Europe is by particles from solid fuel combustion with both residential and urban/industrial origins (Karagulian et al., 2015; Thunis et al., 2018) while biomass burning from wild-fires (Pio et al., 2008) and agricultural fires only contribute marginally in eastern Europe (Stohl et al., 2007). As a result, non-refractory sulfates, primary organic aerosols, and BC are emitted in the atmosphere,

5 leading to average annual concentrations (period including years 2014 to 2018) over Europe of 1.80 µg m^{-3}, 0.94 µg m^{-3}, and 0.23 µg m^{-3} respectively (Yang et al., 2020). However, the types of emission source and aerosol contributions vary seasonally leading to higher aerosol mass concentrations in the wintertime and lower in the summertime (Yang et al., 2020; Chen et al., 2022). Typically, fresh emitted urban/industrial particles are the result of incomplete combustion processes and consist of soot and hydrophobic organic compounds that do not show high hygroscopic growth (Swietlicki et al., 2008). However once in the

10 atmosphere, photochemical aging processes and changes in mixing state (e.g. coating of hydrophilic material) increase particles hygroscopicity (Weingartner et al., 1995; Wang et al., 2010) and their ability to act as CCN (Wittbom et al., 2014). Here, we observed κ_{HTDMA} values almost constant across the measured particle size range of 50 to 250 nm (κ_{HTDMA} values = 0.44, 0.44, 0.49, 0.48, 0.49 respectively for dry particles with D_p = 50, 100, 150, 200, and 250 nm) which suggest the presence of aged, well-mixed particles (Fig. 7f). Mass concentrations of non-refractory sulfate and organics were respectively 1.03 µg m^{-3} and

15 0.50 µg m^{-3}, and almost 3-fold and 5-fold higher than during baseline regime (mean sulfate and organic concentrations in April 2017 = 0.36 µg m^{-3} and 0.11 µg m^{-3} respectively) (Fig. 7h). Furthermore, mean BC concentration = 121 ± 33 ng m^{-3} and up to 176 ng m^{-3} during the time period affected by the transport of particles from Northern Europe, and higher than what was observed during baseline conditions (monthly mean in April 2017 = 36 ± 16 cm^{-3} ng m^{-3}) also confirmed the presence of particles with urban and industrial origins. CO levels were also slightly higher than under baseline conditions ranging between

20 120 and 135 ppb (baseline CO concentration < 112 ppb) indicative of moderately polluted boundary layer (Spackman et al., 2008). Statistically significant increase in N_{tot} baseline regime was observed during the event (mean N_{tot} event = 804 ± 155 cm^{-3} against monthly mean N_{tot} April 2017 = 414 ± 124 cm^{-3}). The Accumulation mode particle concentration was by 3-fold higher during the event than under baseline conditions with the size distribution peaking between 135 and 140 nm, while the increase in N_{At} was statistically significantly lower (= +25%) (Fig. 7g). Consequently, the mean particle diameter shifted toward larger

25 sizes and the contribution of the Accumulation mode to N_{tot} became predominant over the Aitken mode (At contribution = 40 %, Accumulation contribution = 57% corresponding to change in N_{At} / N_{Ac} = 148%). During the event, N_{CCN} exhibited mean values of 179 ± 45 cm^{-3} at SS 0.1% (compared to monthly mean April 2017 = 84 ± 37 cm^{-3}), and 379 ± 23 cm^{-3} at SS 0.2% (compared to monthly mean April 2017 = 122 ± 67 cm^{-3}). The total CCN active fraction was also statistically significant higher during the event than under baseline regime being 30% at SS 0.1%, and = 49% at SS 0.2%, and corresponding to 34% and

30 53% increase at SS 0.1% and SS 0.2% respectively. Accordingly, the slopes of the linear regression between N_{tot} and N_{CCN} are higher during the event than under baseline conditions (at SS 0.1%: N_{CCN} = 0.28N_{tot} and N_{CCN} = 0.19N_{tot} respectively during the event and under baseline conditions, and at SS 0.2%: N_{CCN} = 0.46N_{tot} and N_{CCN} = 0.28N_{tot} during the event and under baseline conditions respectively) indicating the enhanced ability of the continental transported particles to act as CCN (Fig. 7g7i). While comparing the potential activation fraction to the ratio of N_{Ac} and N_{At} the shape of the curves generated were

35 different at SS 0.1% and 0.2% (Fig.7j). A linear regression was generated at SS 0.1% (AF= 0.17 + 0.07N_{Ac}/N_{At}, with r^2 =0.83) versus a lognormal distribution at SS 0.2%. These results suggest that, while at lower supersaturation the number of activated particles was mainly driven by a shift towards larger particle size, at higher supersaturation particle composition also played a strong role. Thus, the increase in N_{CCN} during the event were likely trigged by the combination of high N_{tot}, elevated relative contribution of Accumulation mode particles to N_{tot}, high κ_{HTDMA} values. Supporting our findings, previous studies have

40 hypothesed that shortly after emitted in the atmosphere, sulfate particles mix with BC and other inorganic and organic species. As a consequence, during the transport particles can reach larger D_p and become more hygroscopic due to the presence of sulfate in the mixture, therefore enhancing the CCN active fraction (Swietlicki et al., 2008; Massling et al., 2015).

3.2.3 Multiday transport event of biomass burning aerosols from North America

Pollution and biomass burning aerosols from North America commonly impact the remote North Atlantic region (Honrath, 2004; Alves et al., 2007; Dzepina et al., 2015; García et al., 2017). Zhang et al. (2017) reported that the 16%, 15%, and 13% of the air masses intercepted at Pico Mountain respectively in spring, summer and fall are influenced by North America anthropogenic sources with the 7.3% being associated with wildfire influences. Namely, during summer 2017, several severe wildfires raged in United States and northwest Canada (Kloss et al., 2019). Biomass burning particles in the smoke from the wildfires are typically released and into the lower extratropical stratosphere and transported by cold fronts through the jet stream eastward over the Atlantic Ocean where cold descending airstreams favour their entrainment in the MBL (Owen et al., 2006; Khaykin et al., 2018; Peterson et al., 2018). Here we present a detailed characterization of a long-range transport event of biomass burning aerosols that affected ENA between September 9th and September 13th, 2017. During this period, the arrival of air masses from North America are associated with elevated number of active wildfires in North America and Canada as observed by NASA Worldview VIIRS 375 active fires counts between September 1st and September 15th, 2017. (Fig. 6). Long-range transported biomass burning aerosols from North American and Canadian wildfires at ENA in August 2017 have been also reported by a previous study (Zheng et al., 2020). The presence of biomass burning particles is confirmed by the analysis of aerosol optical properties (data not shown) which shows mean aerosol absorption coefficients at λ 648 nm = 1.04 ± 0.28 Mm^{-1} and mean SSA at λ 464 = 0.93 ± 0.02, in agreement with values reported by previous studies of North American aged wildfire aerosols (Clarke et al., 2007; Zheng et al., 2020), The κ_{HTDMA} values were lower than baseline conditions at 0.32, 0.31, 0.28, 0.28, 0.29 for particles with D_p = 50, 100, 150, 200, and 250 respectively (Fig. 7k), while mean sulfate and organic concentrations were respectively 4-fold and 9-fold higher than under baseline regime (being mean sulfate and organics concentration during the event = 1.75 µg m^{-3} and 4.25 µg m^{-3} respectively, and during the month of September 2017 = 0.4 µg m^{-3} and 0.46 µg m^{-3} respectively) (Fig. 7m). Simultaneously, mean BC concentration were 175 ± 9 ng m^{-3} during the time period affected by the transport of particles from Northern Europe (vs monthly mean BC in August 2017 = 39 ± 22 ng m^{-3}) and mean CO = 186 ± 64 ppb (against mean baseline CO concentration in August 2017 = 94 ± 7 ppb) indicative of moderately polluted boundary layer The substantially elevated concentration of organics and BC particles during the event (up to 8.65 µg m^{-3} and 841 ng m^{-3}) explains the low hygroscopicity of the aerosol particles in the plume, as reported by earlier laboratories studies on aged biomass fuel representative of North American wildfires (Petters et al., 2009; Lathem et al., 2013) (Fig. 7i). The event did not cause a statistically significant increase in particle number concentrations (mean event N_{tot} = 530 ± 189 cm^{-3} compared to monthly mean N_{tot} December 2017 = 421 ± 139 cm^{-3}) which were dominated by particles with D_p > 100 nm (mean Aitken and Accumulation contributions to N_{tot} = 37% and 58% respectively) (fig. 7l). Fresh biomass burning aerosol commonly has an unimodal distribution with D_p between 30 and 100 nm (Hosseini et al., 2010; Levin et al., 2010). However, during the transport events, aerosol processes such as coagulation and condensation of organic material onto existing particles lead to the formation of larger particles with D_p between 170 and 300 nm and to narrower size distribution compared to that of freshly emitted particles (Zellner, 2000; Dentener et al., 2006; Janhäll et al., 2010). Associated to the above-mentioned shift in size distribution, we found potential activation fractions (0.44 and 0.70 at SS 0.1% and 70% at SS at 0.2%, respectively) approximately twice that under baseline conditions, suggesting that . the transported aerosol particles are more effective as CCN. . Similarly, the r^2 and slopes obtained through linear regression between N_{tot} and N_{CCN} are higher under periods affected by the events compared to baseline conditions (r^2 = 0.56 with a slope of 0.44 ± 0.005 at SS 0.1% and r^2 = 0.66 with a slope of 0.68 ± 0.007 at SS 0.2% during the event, against r^2 = 0.32 with a slope of 0.22 ± 0.001 at SS 0.1% and r^2 = 0.40 with a slope of 0.34 ± 0.007 at SS 0.2%) (Fig. 7n). The CCN concentration was higher (respectively 220% at SS 0.1%, and 227% at SS 0.2%) during the event then for rest of the month of September 2017. Furthermore, comparing the potential activation fraction to the ratio of N_{Ac} and N_{At} we obtained lognormal distributions at both SS 0.1% and SS 0.2% indicating that particle composition also affect the concentration of particles that can act as CCN (Fig. 7o). These results demonstrate that aged wildfire aerosols

dominate the accumulation mode and act better as CCN and affect CCN budget at ENA with potential effects on Earth's albedo, clouds lifetime and precipitation (Albrecht, 1989).

3.2.4 Continental aerosol influences on regional aerosols properties and CCN

5   Multiday aerosol plume transport events at ENA influence regional aerosol properties and CCN concentrations. However, the extent of changes in N_{tot} and particle size mode are dependent on the origin and composition of the transported particles and affects CCN concentrations differently. Here, we provide a summary statistic of the influence of continental aerosol emissions on baseline aerosol population and baseline CCN concentrations at ENA for the three multiday event regimes discussed in Section 3.2.

10   The arrival of mixture of marine aerosol and dust plumes as observed in the months of March, 2017 with Arctic and Canada origins, and in November, and December 2017 originated in North Africa, cause provoked statistically significant increase in N_{tot} (123%), accompanied by statistically non-significant shifts in size distribution and CCN potential activation fraction (Fig 8a). Namely, particle concentrations in the Aitken and Accumulation mode show comparable increase (mean increase = 117% and 146% respectively for N_{At} and N_{Ac}) (Fig. 8a), and consequently the relative Aitken and Accumulation mode contributions to N_{tot} remain almost constant (N_{At} / N_{Ac} changes < 1%), with the mean Aitken and Accumulation modes being respectively 59% and 38% of the total number concentration (Fig. 8b) and similar to the baseline condition (where At mode contributes 61% and Accumulation mode 36% to N_{tot}) (Fig. 8b). The gravitational settling of coarse particle during the transport to ENA is likely the reason why we did not find statistically significant shifts towards larger particle sizes (Lawrence and Neff, 2009; Mahowald et al., 2014; Friese et al., 2016). Although wet scavenging might also played a role in the removal of coarse particles.

20   The arrival of the aerosol plumes at ENA also lead to higher CCN concentrations (mean increase = 122% and 162% respectively at SS 0.1% and SS 0.2%) than under unperturbed aerosol regime. However, these increases were not accompanied by statistically significant changes in CCN potential activation fractions which remained similar to the baseline conditions during the entire duration of the event (mean AF during the event: $AF_{0.1\%}$ = 0.26 and $AF_{0.2\%}$ = 0.42 against mean AF under unperturbed aerosol conditions: $AF_{0.1\%}$ = 0.27 and $AF_{0.2\%}$ = 0.41) (Fig. 8a). These results indicate that mixture of dust and marine aerosol particles have the same ability of acting as CCN that marine regional aerosol at ENA have, and the elevated N_{CCN} are a consequence of increased N_{tot}.

The multiday aerosol plume transport events that occurred in the months of January, April, May, and October of 2017, dominated by a mixture of marine and polluted continental aerosol and originated in continental industrialized areas such as Northern Europe, and North America, caused statistically significant changes in baseline submicron particle number concentration, size distribution, and CCN potential activation fraction. Furthermore, we found ~ 4-fold higher aerosol absorption coefficient at 648 nm and mean absorption Angstrom exponent at λ 460/648 nm =1.04 ± 0.1 Mm^{-1} during the events, and mean black carbon concentration was = 177 ± 76 ng m^{-3} and up to 319 ng m^{-3} against mean concentration under unperturbed aerosol conditions of 35 ± 16 ng m^{-3} (data not shown), as expected for aerosol with enhanced contribution from fossil fuel and urban pollution sources (Clarke et al., 2007; Cazorla et al., 2013). During the events, the number concentration of submicron particles at ENA experienced a mean increase of 108% due to 37% and 256% mean increases respectively in the N_{At} and N_{Ac} modes (and corresponding to N_{At} / N_{Ac} changes > 200%) (Fig. 8a). Therefore, the Accumulation mode became predominant over the Aitken mode. Namely, during multiday aerosol plume transport events the average contributions of the Aitken mode to the total number particle concentrations was 42% (between 35% and 45% depending on the event), while the average contributions of the Accumulation mode to N_{tot} was 56% (between 45% and 60%) (Fig. 8b). The aforementioned changes in baseline aerosol regime in terms of number particle concentrations and shifts in size distributions caused higher CCN concentrations (mean increase = 176% and 240% respectively at SS 0.1% and SS 0.2%) and statistically significant

increases in CCN potential activation fractions (mean AF during the event: $AF_{0.1\%} = 0.34$ and $AF_{0.2\%} = 0.55$ corresponding to AF increases between 25% and 50%) (Fig. 8a). This result suggests that polluted particles of continental origins with $D_p > 100$ nm are sufficiently large to readily serve as CCN, and have the potential to substantially increase CCN concentrations in marine remote regions (Hudson and Xie, 1999).

5 Finally, the long-range transport of smoke and biomass burning aerosols identified in months of August and September 2017 did not impact the concentration of submicron aerosol particles, causing only a weak increase (< +25%) in submicron number particle concentrations. However, the events led to statistically significant shifts in particle size distribution and an increase in the CCN potential activation fraction respect to baseline conditions, namely these events caused only a weak increase (< +25%) in submicron number particle concentrations accompanied by the decrease of Aitken mode particle concentrations (mean

10 reduction = -39% and down to -50%) and increase of Accumulation mode particle concentrations (mean increase = +115%) (Fig. 6i, j). Thus, during the High CCN activation events, Aitken mode particles only represented 33% of Ntot, while mean Accumulation mode contribution to N_{tot} was = 63% (Fig. 8b). The shift in size distribution corresponded to a decrease in the N_{At}/N_{Ac} ratio of ~300%. Simultaneously, mean CCN concentrations and AF values were 118% and 119% higher during the event compared to baseline conditions at SS of 0.1% and 0.2% respectively, and associated with elevated mean CCN potential

15 activation fraction (= 0.46 at SS 0.1%, and 0.74 at SS 0.2) (Fig. 8a). These findings suggest that the shape of the submicron particle size distribution exerts a considerable effect on the ability of aerosol to act as CCN, and the arrival of biomass burning aerosols from continental wildfires statistically significantly affects the CCN concentrations at ENA.

4. Conclusions

20 Multiday aerosol events due to long-range transport of continental aerosols, are observed at ENA throughout the year. In this study we develop an algorithm that integrates submicron aerosol size distribution, single scattering albedo and black carbon concentration measurements to identify multiday aerosol plume transport events occurring at ENA in 2017. In the year 2017, we identified nine events of long-range transported particles (with durations >24 hours), corresponding to ~7.5% of the year. Analysis of 10-day HYSPLIT backward trajectories and CALIPSO aerosol products indicate different origins and aerosol

25 compositions of the air masses arriving at ENA during the transport events. Namely, we observe the arrival of 1) mixture of dust and marine aerosols from the Arctic and Canada in March 2017 and from North Africa in November and December 2017, 2) a mixture of marine and polluted continental aerosols from Northern Europe and North America in January, April, May, and October 2017, and 3) pollution and biomass burning aerosol from North America and Canada in the months of August and September 2017. Subsequently, we assess the influence of aerosol plumes composition on CCN concentrations at ENA,

30 investigating the mechanisms that trigger the increase in N_{CCN}. The events characterized by the arrival of mixture of dust and marine aerosols at ENA caused statistically significant increases in N_{tot}, while the aerosol size distribution and CCN potential activation fraction remained similar to baseline conditions, indicating that greater N_{CCN} were attributable to the elevated concentration of particles during the event. High CCN concentrations are attributed to both high N_{tot}, and dominance of particles large enough to act as CCN ($D_p > 100$ nm) from mixed marine and polluted continental aerosol plumes. Conversely,

35 despite only causing slight increases in baseline N_{tot}, the events dominated by the arrival of biomass burning aerosols were characterized by the presence of particles with strong ability to act as CCN leading to two-fold higher N_{CCN}. Based on our analysis, the transport of continental particles at ENA, caused a total N_{CCN} increase by ~22% respect to CCN baseline regime, impacting ~28 days, and strongly contributing to the CCN concentrations at ENA in 2017. Namely, we observed that plumes dominated by mixture of dust and marine aerosols, mixture of marine and polluted continental aerosols, and biomass burning

40 aerosols can cause respectively 6.5%, 8%, and 7.4% increase in N_{CCN}. Furthermore, we showed that, once the multiday aerosol event is identified, the analysis of changes in baseline N_{tot} and particle size distribution as well as their correlation, might be used as proxy to estimate how CCN is affected. Based on the characteristics of the type events discussed above, in the future

an algorithm to predict N_{CCN} variations during multiday events of long-range transport of aerosols could be developed and validateed at ENA to inform study at other locations and constrain model predictions of CCN regime perturbations over remote oceans. Furthermore, the influences of aerosol perturbations on cloud properties and cloud adjustment at ENA might be explore in future studies using ARM retrieved cloud optical properties value-added products as well as ARM ceilometer lidar and

5 KAZR2 datasets upon evaluations of radar-lidar techniques and validation of retrieved observations against in situ measurements.

10 Data availability: data were obtained from the Atmospheric Radiation Measurement (ARM) User Facility, a U.S. Department of Energy Office of Science user facility sponsored by the Office of Biological and Environmental Research (available at https://www.archive.arm.gov/discovery).

Competing interest: The authors declare that they have no conflicts of interest.

15 Acknowledgements: The work was supported by the Atmospheric Radiation Measurement (ARM) program, funded by the U.S. Department of Energy (DOE), Office of Science, Office of Biological and Environmental Research. We acknowledge the ARM Research Facility, a user facility of the U.S. DOE, Office of Science, sponsored by the Office of Biological and Environmental Research for providing data. Robert Wood acknowledges funding from ASR award DE-SC0021103. We acknowledge the use of data and/or imagery from NASA's Fire Information for Resource Management System (FIRMS)

20 (https://earthdata.nasa.gov/firms), part of NASA's Earth Observing System Data and Information System (EOSDIS). We also acknowledge the ENA ARM Site Operators, Carlos Sousa, Tercio Silva and Bruno Cunha.

References

Aiken, A., Gallo, F., Uin, J., Springston, S., Wang, J., Zheng, G., Kuang, C., McComiskey, A., Wood, R., Flynn, C., Theisen, A., Azevedo, E., Ortega, P., and Powers, H.: Eastern North Atlantic (ENA) Aerosol Supplementary Site (S1) Data Analysis Report, https://doi.org/10.2172/1567063, 2019.

5 Albrecht, B. A.: Aerosols, Cloud Microphysics, and Fractional Cloudiness, Science, 245, 1227–1230, https://doi.org/10.1126/science.245.4923.1227, 1989.

Albrecht, B. A., Bretherton, C. S., Johnson, D., Scubert, W. H., and Frisch, A. S.: The Atlantic Stratocumulus Transition Experiment—ASTEX, Bull. Am. Meteorol. Soc., 76, 889–904, https://doi.org/10.1175/1520-0477(1995)076<0889:TASTE>2.0.CO;2, 1995.

10 Alonso-Pérez, S., Cuevas, E., Querol, X., Viana, M., and Guerra, J. C.: Impact of the Saharan dust outbreaks on the ambient levels of total suspended particles (TSP) in the marine boundary layer (MBL) of the Subtropical Eastern North Atlantic Ocean, Atmos. Environ., 41, 9468–9480, https://doi.org/10.1016/j.atmosenv.2007.08.049, 2007.

Alonso-Perez, S., Cuevas, E., Perez, C., Querol, X., Baldasano, J. M., Draxler, R., and De Bustos, J. J.: Trend changes of African airmass intrusions in the marine boundary layer over the subtropical Eastern North Atlantic region in winter: TREND
15 CHANGES OF AFRICAN AIRMASS INTRUSIONS, Tellus B, 63, 255–265, https://doi.org/10.1111/j.1600-0889.2010.00524.x, 2011.

Alves, C., Oliveira, T., Pio, C., Silvestre, A. J. D., Fialho, P., Barata, F., and Legrand, M.: Characterisation of carbonaceous aerosols from the Azorean Island of Terceira, Atmos. Environ., 41, 1359–1373, https://doi.org/10.1016/j.atmosenv.2006.10.022, 2007.

20 Andreae, M. O., Andreae, T. W., Meyerdierks, D., and Thiel, C.: Marine sulfur cycling and the atmospheric aerosol over the springtime North Atlantic, Chemosphere, 52, 1321–1343, https://doi.org/10.1016/S0045-6535(03)00366-7, 2003.

Astitha, M., Kallos, G., Spyrou, C., O'Hirok, W., Lelieveld, J., and Denier van der Gon, H. A. C.: Modelling the chemically aged and mixed aerosols over the eastern central Atlantic Ocean – potential impacts, Atmospheric Chem. Phys., 10, 5797–5822, https://doi.org/10.5194/acp-10-5797-2010, 2010.

25 Bates, T. S., Kapustin, V. N., Quinn, P. K., Covert, D. S., Coffman, D. J., Mari, C., Durkee, P. A., De Bruyn, W. J., and Saltzman, E. S.: Processes controlling the distribution of aerosol particles in the lower marine boundary layer during the First Aerosol Characterization Experiment (ACE 1), J. Geophys. Res. Atmospheres, 103, 16369–16383, https://doi.org/10.1029/97JD03720, 1998.

Behrenfeld, M. J., Moore, R. H., Hostetler, C. A., Graff, J., Gaube, P., Russell, L. M., Chen, G., Doney, S. C., Giovannoni, S.,
30 Liu, H., Proctor, C., Bolaños, L. M., Baetge, N., Davie-Martin, C., Westberry, T. K., Bates, T. S., Bell, T. G., Bidle, K. D., Boss, E. S., Brooks, S. D., Cairns, B., Carlson, C., Halsey, K., Harvey, E. L., Hu, C., Karp-Boss, L., Kleb, M., Menden-Deuer, S., Morison, F., Quinn, P. K., Scarino, A. J., Anderson, B., Chowdhary, J., Crosbie, E., Ferrare, R., Hair, J. W., Hu, Y., Janz, S., Redemann, J., Saltzman, E., Shook, M., Siegel, D. A., Wisthaler, A., Martin, M. Y., and Ziemba, L.: The North Atlantic Aerosol and Marine Ecosystem Study (NAAMES): Science Motive and Mission Overview, Front. Mar. Sci., 6, 122,
35 https://doi.org/10.3389/fmars.2019.00122, 2019.

Ben-Ami, Y., Koren, I., and Altaratz, O.: Patterns of North African dust transport over the Atlantic: winter vs. summer, based on CALIPSO first year data, Atmospheric Chem. Phys., 9, 7867–7875, https://doi.org/10.5194/acp-9-7867-2009, 2009.

Bond, T. C. and Bergstrom, R. W.: Light Absorption by Carbonaceous Particles: An Investigative Review, Aerosol Sci. Technol., 40, 27–67, https://doi.org/10.1080/02786820500421521, 2006.

40 Bond, T. C., Anderson, T. L., and Campbell, D.: Calibration and Intercomparison of Filter-Based Measurements of Visible Light Absorption by Aerosols, Aerosol Sci. Technol., 30, 582–600, https://doi.org/10.1080/027868299304435, 1999.

Bony, S.: Marine boundary layer clouds at the heart of tropical cloud feedback uncertainties in climate models, Geophys. Res. Lett., 32, L20806, https://doi.org/10.1029/2005GL023851, 2005.

Bressi, M., Cavalli, F., Putaud, J. P., Fröhlich, R., Petit, J.-E., Aas, W., Äijälä, M., Alastuey, A., Allan, J. D., Aurela, M.,
45 Berico, M., Bougiatioti, A., Bukowiecki, N., Canonaco, F., Crenn, V., Dusanter, S., Ehn, M., Elsasser, M., Flentje, H., Graf, P., Green, D. C., Heikkinen, L., Hermann, H., Holzinger, R., Hueglin, C., Keernik, H., Kiendler-Scharr, A., Kubelová, L., Lunder, C., Maasikmets, M., Makeš, O., Malaguti, A., Mihalopoulos, N., Nicolas, J. B., O'Dowd, C., Ovadnevaite, J., Petralia, E., Poulain, L., Priestman, M., Riffault, V., Ripoll, A., Schlag, P., Schwarz, J., Sciare, J., Slowik, J., Sosedova, Y., Stavroulas,

I., Teinemaa, E., Via, M., Vodička, P., Williams, P. I., Wiedensohler, A., Young, D. E., Zhang, S., Favez, O., Minguillón, M. C., and Prevot, A. S. H.: A European aerosol phenomenology - 7: High-time resolution chemical characteristics of submicron particulate matter across Europe, Atmospheric Environ. X, 10, 100108, https://doi.org/10.1016/j.aeaoa.2021.100108, 2021.

5 Bullard, J. E., Baddock, M., Bradwell, T., Crusius, J., Darlington, E., Gaiero, D., Gassó, S., Gisladottir, G., Hodgkins, R., McCulloch, R., McKenna-Neuman, C., Mockford, T., Stewart, H., and Thorsteinsson, T.: High-latitude dust in the Earth system, Rev. Geophys., 54, 447–485, https://doi.org/10.1002/2016RG000518, 2016.

Bullard, R. L., Kuang, C., Uin, J., Smith, S., and Springston, S. R.: Aerosol Inlet Characterization Experiment Report, https://doi.org/10.2172/1355300, 2017.

Burton, S. P., Ferrare, R. A., Vaughan, M. A., Omar, A. H., Rogers, R. R., Hostetler, C. A., and Hair, J. W.: Aerosol
10 classification from airborne HSRL and comparisons with the CALIPSO vertical feature mask, Atmospheric Meas. Tech., 6, 1397–1412, https://doi.org/10.5194/amt-6-1397-2013, 2013.

Carslaw, K. S., Lee, L. A., Reddington, C. L., Pringle, K. J., Rap, A., Forster, P. M., Mann, G. W., Spracklen, D. V., Woodhouse, M. T., Regayre, L. A., and Pierce, J. R.: Large contribution of natural aerosols to uncertainty in indirect forcing, Nature, 503, 67–71, https://doi.org/10.1038/nature12674, 2013.

15 Cavalli, F., Alastuey, A., Areskoug, H., Ceburnis, D., Čech, J., Genberg, J., Harrison, R. M., Jaffrezo, J. L., Kiss, G., Laj, P., Mihalopoulos, N., Perez, N., Quincey, P., Schwarz, J., Sellegri, K., Spindler, G., Swietlicki, E., Theodosi, C., Yttri, K. E., Aas, W., and Putaud, J. P.: A European aerosol phenomenology -4: Harmonized concentrations of carbonaceous aerosol at 10 regional background sites across Europe, Atmos. Environ., 144, 133–145, https://doi.org/10.1016/j.atmosenv.2016.07.050, 2016.

20 Cazorla, A., Bahadur, R., Suski, K. J., Cahill, J. F., Chand, D., Schmid, B., Ramanathan, V., and Prather, K. A.: Relating aerosol absorption due to soot, organic carbon, and dust to emission sources determined from in-situ chemical measurements, Atmospheric Chem. Phys., 13, 9337–9350, https://doi.org/10.5194/acp-13-9337-2013, 2013.

Charlson, R. J., Lovelock, J. E., Andreae, M. O., and Warren, S. G.: Oceanic phytoplankton, atmospheric sulphur, cloud albedo and climate, Nature, 326, 655–661, https://doi.org/10.1038/326655a0, 1987.

25 Chen, G., Canonaco, F., Tobler, A., Aas, W., Alastuey, A., Allan, J., Atabakhsh, S., Aurela, M., Baltensperger, U., Bougiatioti, A., De Brito, J. F., Ceburnis, D., Chazeau, B., Chebaicheb, H., Daellenbach, K. R., Ehn, M., El Haddad, I., Eleftheriadis, K., Favez, O., Flentje, H., Font, A., Fossum, K., Freney, E., Gini, M., Green, D. C., Heikkinen, L., Herrmann, H., Kalogridis, A.-C., Keernik, H., Lhotka, R., Lin, C., Lunder, C., Maasikmets, M., Manousakas, M. I., Marchand, N., Marin, C., Marmureanu, L., Mihalopoulos, N., Močnik, G., Nęcki, J., O'Dowd, C., Ovadnevaite, J., Peter, T., Petit, J.-E., Pikridas, M., Matthew Platt,
30 S., Pokorná, P., Poulain, L., Priestman, M., Riffault, V., Rinaldi, M., Różański, K., Schwarz, J., Sciare, J., Simon, L., Skiba, A., Slowik, J. G., Sosedova, Y., Stavroulas, I., Styszko, K., Teinemaa, E., Timonen, H., Tremper, A., Vasilescu, J., Via, M., Vodička, P., Wiedensohler, A., Zografou, O., Cruz Minguillón, M., and Prévôt, A. S. H.: European aerosol phenomenology − 8: Harmonised source apportionment of organic aerosol using 22 Year-long ACSM/AMS datasets, Environ. Int., 166, 107325, https://doi.org/10.1016/j.envint.2022.107325, 2022.

35 Chiapello, I.: Understanding the long-term variability of African dust transport across the Atlantic as recorded in both Barbados surface concentrations and large-scale Total Ozone Mapping Spectrometer (TOMS) optical thickness, J. Geophys. Res., 110, D18S10, https://doi.org/10.1029/2004JD005132, 2005.

China, S., Scarnato, B., Owen, R. C., Zhang, B., Ampadu, M. T., Kumar, S., Dzepina, K., Dziobak, M. P., Fialho, P., Perlinger, J. A., Hueber, J., Helmig, D., Mazzoleni, L. R., and Mazzoleni, C.: Morphology and mixing state of aged soot particles at a
40 remote marine free troposphere site: Implications for optical properties, Geophys. Res. Lett., 42, 1243–1250, https://doi.org/10.1002/2014GL062404, 2015.

Choobari, O. A., Zawar-Reza, P., and Sturman, A.: The global distribution of mineral dust and its impacts on the climate system: A review, Atmospheric Res., 138, 152–165, https://doi.org/10.1016/j.atmosres.2013.11.007, 2014.

Clarke, A. and Kapustin, V.: Hemispheric Aerosol Vertical Profiles: Anthropogenic Impacts on Optical Depth and Cloud
45 Nuclei, Science, 329, 1488–1492, https://doi.org/10.1126/science.1188838, 2010.

Clarke, A., McNaughton, C., Kapustin, V., Shinozuka, Y., Howell, S., Dibb, J., Zhou, J., Anderson, B., Brekhovskikh, V., Turner, H., and Pinkerton, M.: Biomass burning and pollution aerosol over North America: Organic components and their influence on spectral optical properties and humidification response, J. Geophys. Res., 112, D12S18, https://doi.org/10.1029/2006JD007777, 2007.

Cooke, W. F., Jennings, S. G., and Spain, T. G.: Black carbon measurements at Mace Head, 1989-1996, J. Geophys. Res. Atmospheres, 102, 25339–25346, https://doi.org/10.1029/97JD01430, 1997.

Costabile, F., Barnaba, F., Angelini, F., and Gobbi, G. P.: Identification of key aerosol populations through their size and composition resolved spectral scattering and absorption, Atmospheric Chem. Phys., 13, 2455–2470, https://doi.org/10.5194/acp-13-2455-2013, 2013.

Cuevas, E., Gómez-Peláez, A. J., Rodríguez, S., Terradellas, E., Basart, S., García, R. D., García, O. E., and Alonso-Pérez, S.: The pulsating nature of large-scale Saharan dust transport as a result of interplays between mid-latitude Rossby waves and the North African Dipole Intensity, Atmos. Environ., 167, 586–602, https://doi.org/10.1016/j.atmosenv.2017.08.059, 2017.

Dadashazar, H., Painemal, D., Alipanah, M., Brunke, M., Chellappan, S., Corral, A. F., Crosbie, E., Kirschler, S., Liu, H., Moore, R. H., Robinson, C., Scarino, A. J., Shook, M., Sinclair, K., Thornhill, K. L., Voigt, C., Wang, H., Winstead, E., Zeng, X., Ziemba, L., Zuidema, P., and Sorooshian, A.: Cloud drop number concentrations over the western North Atlantic Ocean: seasonal cycle, aerosol interrelationships, and other influential factors, Atmospheric Chem. Phys., 21, 10499–10526, https://doi.org/10.5194/acp-21-10499-2021, 2021.

Dentener, F., Kinne, S., Bond, T., Boucher, O., Cofala, J., Generoso, S., Ginoux, P., Gong, S., Hoelzemann, J. J., Ito, A., Marelli, L., Penner, J. E., Putaud, J.-P., Textor, C., Schulz, M., van der Werf, G. R., and Wilson, J.: Emissions of primary aerosol and precursor gases in the years 2000 and 1750 prescribed data-sets for AeroCom, Atmospheric Chem. Phys., 6, 4321–4344, https://doi.org/10.5194/acp-6-4321-2006, 2006.

Dong, X., Xi, B., Kennedy, A., Minnis, P., and Wood, R.: A 19-Month Record of Marine Aerosol–Cloud–Radiation Properties Derived from DOE ARM Mobile Facility Deployment at the Azores. Part I: Cloud Fraction and Single-Layered MBL Cloud Properties, J. Clim., 27, 3665–3682, https://doi.org/10.1175/JCLI-D-13-00553.1, 2014.

Dzepina, K., Mazzoleni, C., Fialho, P., China, S., Zhang, B., Owen, R. C., Helmig, D., Hueber, J., Kumar, S., Perlinger, J. A., Kramer, L. J., Dziobak, M. P., Ampadu, M. T., Olsen, S., Wuebbles, D. J., and Mazzoleni, L. R.: Molecular characterization of free tropospheric aerosol collected at the Pico Mountain Observatory: a case study with a long-range transported biomass burning plume, Atmospheric Chem. Phys., 15, 5047–5068, https://doi.org/10.5194/acp-15-5047-2015, 2015.

Facchini, M. C., Rinaldi, M., Decesari, S., Carbone, C., Finessi, E., Mircea, M., Fuzzi, S., Ceburnis, D., Flanagan, R., Nilsson, E. D., de Leeuw, G., Martino, M., Woeltjen, J., and O'Dowd, C. D.: Primary submicron marine aerosol dominated by insoluble organic colloids and aggregates, Geophys. Res. Lett., 35, L17814, https://doi.org/10.1029/2008GL034210, 2008.

Fan, J., Wang, Y., Rosenfeld, D., and Liu, X.: Review of Aerosol–Cloud Interactions: Mechanisms, Significance, and Challenges, J. Atmospheric Sci., 73, 4221–4252, https://doi.org/10.1175/JAS-D-16-0037.1, 2016.

Feingold, G. and McComiskey, A.: ARM's Aerosol–Cloud–Precipitation Research (Aerosol Indirect Effects), Meteorol. Monogr., 57, 22.1-22.15, https://doi.org/10.1175/AMSMONOGRAPHS-D-15-0022.1, 2016.

Formenti, P., Elbert, W., Maenhaut, W., Haywood, J. M., and Andreae, M. O.: Chemical composition of mineral dust aerosol during the Saharan Dust Experiment (SHADE) airborne campaign in the Cape Verde region, September 2000, J. Geophys. Res., 108, 8576, https://doi.org/10.1029/2002JD002648, 2003.

Friese, C. A., van der Does, M., Merkel, U., Iversen, M. H., Fischer, G., and Stuut, J.-B. W.: Environmental factors controlling the seasonal variability in particle size distribution of modern Saharan dust deposited off Cape Blanc, Aeolian Res., 22, 165–179, https://doi.org/10.1016/j.aeolia.2016.04.005, 2016.

Gallo, F. and Aiken, A. C.: EASTERN NORTH ATLANTIC (ENA) CONDENSATION PARTICLE COUNTER (CPC) with the AEROSOL MASK (ENA-AM) for the YEAR 2017, 2022.

Gallo, F., Uin, J., Springston, S., Wang, J., Zheng, G., Kuang, C., Wood, R., Azevedo, E. B., McComiskey, A., Mei, F., Theisen, A., Kyrouac, J., and Aiken, A. C.: Identifying a regional aerosol baseline in the eastern North Atlantic using collocated measurements and a mathematical algorithm to mask high-submicron-number-concentration aerosol events, Atmospheric Chem. Phys., 20, 7553–7573, https://doi.org/10.5194/acp-20-7553-2020, 2020a.

Gallo, F., Uin, J., Springston, S., Wang, J., Zheng, G., Kuang, C., Wood, R., Azevedo, E. B., McComiskey, A., Mei, F., Theisen, A., Kyrouac, J., and Aiken, A. C.: Identifying a regional aerosol baseline in the eastern North Atlantic using collocated measurements and a mathematical algorithm to mask high-submicron-number-concentration aerosol events, Atmospheric Chem. Phys., 20, 7553–7573, https://doi.org/10.5194/acp-20-7553-2020, 2020b.

Gallo, F., Sanchez, K. J., Anderson, B. E., Bennett, R., Brown, M. D., Crosbie, E. C., Hostetler, C., Jordan, C., Yang Martin, M., Robinson, C. E., Russell, L. M., Shingler, T. J., Shook, M. A., Thornhill, K. L., Wiggins, E. B., Winstead, E. L., Wisthaler,

A., Ziemba, L. D., and Moore, R. H.: Measurement report: Aerosol vertical profiles over the Western North Atlantic Ocean during the North Atlantic Aerosols and Marine Ecosystems Study (NAAMES), Aerosols/Field Measurements/Troposphere/Chemistry (chemical composition and reactions), https://doi.org/10.5194/acp-2022-654, 2022.

Gao, S., Lu, C., Liu, Y., Mei, F., Wang, J., Zhu, L., and Yan, S.: Contrasting Scale Dependence of Entrainment-Mixing Mechanisms in Stratocumulus Clouds, Geophys. Res. Lett., 47, https://doi.org/10.1029/2020GL086970, 2020.

García, M. I., Rodríguez, S., and Alastuey, A.: Impact of North America on the aerosol composition in the North Atlantic free troposphere, Atmospheric Chem. Phys., 17, 7387–7404, https://doi.org/10.5194/acp-17-7387-2017, 2017.

Garrett, T. J. and Hobbs, P. V.: Long-Range Transport of Continental Aerosols over the Atlantic Ocean and Their Effects on Cloud Structures, J. Atmospheric Sci., 52, 2977–2984, https://doi.org/10.1175/1520-0469(1995)052<2977:LRTOCA>2.0.CO;2, 1995.

Giangrande, S. E., Wang, D., Bartholomew, M. J., Jensen, M. P., Mechem, D. B., Hardin, J. C., and Wood, R.: Midlatitude Oceanic Cloud and Precipitation Properties as Sampled by the ARM Eastern North Atlantic Observatory, J. Geophys. Res. Atmospheres, 124, 4741–4760, https://doi.org/10.1029/2018JD029667, 2019.

Haynes, W.: Tukey's Test, in: Encyclopedia of Systems Biology, edited by: Dubitzky, W., Wolkenhauer, O., Cho, K.-H., and Yokota, H., Springer New York, New York, NY, 2303–2304, https://doi.org/10.1007/978-1-4419-9863-7_1212, 2013.

Honrath, R. E.: Regional and hemispheric impacts of anthropogenic and biomass burning emissions on summertime CO and O_3 in the North Atlantic lower free troposphere, J. Geophys. Res., 109, D24310, https://doi.org/10.1029/2004JD005147, 2004.

Honrath, R. E., Owen, R. C., Val Martín, M., Seid, J. S., Lapina, K., Fialho, P., Dziobak, M. P., Kleissl, J., and Westphal, D. L.: Regional and hemispheric impacts of anthropogenic and biomass burning emissions on summertime CO and O_3 in the North Atlantic lower free troposphere, J. Geophys. Res., 109, D24310, https://doi.org/10.1029/2004JD005147, 2004.

Hosseini, S., Li, Q., Cocker, D., Weise, D., Miller, A., Shrivastava, M., Miller, J. W., Mahalingam, S., Princevac, M., and Jung, H.: Particle size distributions from laboratory-scale biomass fires using fast response instruments, Atmospheric Chem. Phys., 10, 8065–8076, https://doi.org/10.5194/acp-10-8065-2010, 2010.

Hudson, J. G. and Xie, Y.: Vertical distributions of cloud condensation nuclei spectra over the summertime northeast Pacific and Atlantic Oceans, J. Geophys. Res. Atmospheres, 104, 30219–30229, https://doi.org/10.1029/1999JD900413, 1999.

Janhäll, S., Andreae, M. O., and Pöschl, U.: Biomass burning aerosol emissions from vegetation fires: particle number and mass emission factors and size distributions, Atmospheric Chem. Phys., 10, 1427–1439, https://doi.org/10.5194/acp-10-1427-2010, 2010.

Junker, C., Jennings, S. G., and Cachier, H.: Aerosol light absorption in the North Atlantic: trends and seasonal characteristics during the period 1989 to 2003, Atmospheric Chem. Phys., 6, 1913–1925, https://doi.org/10.5194/acp-6-1913-2006, 2006.

Kalashnikova, O. V. and Kahn, R. A.: Mineral dust plume evolution over the Atlantic from MISR and MODIS aerosol retrievals, J. Geophys. Res., 113, D24204, https://doi.org/10.1029/2008JD010083, 2008.

Kallos, G., Astitha, M., Katsafados, P., and Spyrou, C.: Long-Range Transport of Anthropogenically and Naturally Produced Particulate Matter in the Mediterranean and North Atlantic: Current State of Knowledge, J. Appl. Meteorol. Climatol., 46, 1230–1251, https://doi.org/10.1175/JAM2530.1, 2007.

Karagulian, F., Belis, C. A., Dora, C. F. C., Prüss-Ustün, A. M., Bonjour, S., Adair-Rohani, H., and Amann, M.: Contributions to cities' ambient particulate matter (PM): A systematic review of local source contributions at global level, Atmos. Environ., 120, 475–483, https://doi.org/10.1016/j.atmosenv.2015.08.087, 2015.

Khaykin, S. M., Godin-Beekmann, S., Hauchecorne, A., Pelon, J., Ravetta, F., and Keckhut, P.: Stratospheric Smoke With Unprecedentedly High Backscatter Observed by Lidars Above Southern France, Geophys. Res. Lett., 45, 1639–1646, https://doi.org/10.1002/2017GL076763, 2018.

Kleefeld, C.: Relative contribution of submicron and supermicron particles to aerosol light scattering in the marine boundary layer, J. Geophys. Res., 107, 8103, https://doi.org/10.1029/2000JD000262, 2002.

Kloss, C., Berthet, G., Sellitto, P., Ploeger, F., Bucci, S., Khaykin, S., Jégou, F., Taha, G., Thomason, L. W., Barret, B., Le Flochmoen, E., von Hobe, M., Bossolasco, A., Bègue, N., and Legras, B.: Transport of the 2017 Canadian wildfire plume to the tropics via the Asian monsoon circulation, Atmospheric Chem. Phys., 19, 13547–13567, https://doi.org/10.5194/acp-19-13547-2019, 2019.

Koehler, K. A., Kreidenweis, S. M., DeMott, P. J., Petters, M. D., Prenni, A. J., and Carrico, C. M.: Hygroscopicity and cloud droplet activation of mineral dust aerosol, Geophys. Res. Lett., 36, L08805, https://doi.org/10.1029/2009GL037348, 2009.

Kolstad, E. W., Bracegirdle, T. J., and Seierstad, I. A.: Marine cold-air outbreaks in the North Atlantic: temporal distribution and associations with large-scale atmospheric circulation, Clim. Dyn., 33, 187–197, https://doi.org/10.1007/s00382-008-0431-5, 2009.

Korhonen, H., Carslaw, K. S., Spracklen, D. V., Mann, G. W., and Woodhouse, M. T.: Influence of oceanic dimethyl sulfide emissions on cloud condensation nuclei concentrations and seasonality over the remote Southern Hemisphere oceans: A global model study, J. Geophys. Res., 113, D15204, https://doi.org/10.1029/2007JD009718, 2008.

Korolev, A. V. and Mazin, I. P.: Supersaturation of Water Vapor in Clouds, J. Atmospheric Sci., 60, 2957–2974, https://doi.org/10.1175/1520-0469(2003)060<2957:SOWVIC>2.0.CO;2, 2003.

Kuang, C., Mei, F., Pacific Northwest National Laboratory, Brookhaven National Laboratory, Argonne National Laboratory, and Oak Ridge National Laboratory: Condensation Particle Counter (CPC) Instrument Handbook - Airborne Version, https://doi.org/10.2172/1562676, 2019.

Laken, B. A., Parviainen, H., Pallé, E., and Shahbaz, T.: Saharan mineral dust outbreaks observed over the North Atlantic island of La Palma in summertime between 1984 and 2012: Summertime Saharan Dust Outbreaks over La Palma, Q. J. R. Meteorol. Soc., 140, 1058–1068, https://doi.org/10.1002/qj.2170, 2014.

Lapina, K., Heald, C. L., Spracklen, D. V., Arnold, S. R., Allan, J. D., Coe, H., McFiggans, G., Zorn, S. R., Drewnick, F., Bates, T. S., Hawkins, L. N., Russell, L. M., Smirnov, A., O'Dowd, C. D., and Hind, A. J.: Investigating organic aerosol loading in the remote marine environment, Atmospheric Chem. Phys., 11, 8847–8860, https://doi.org/10.5194/acp-11-8847-2011, 2011.

Lathem, T. L., Beyersdorf, A. J., Thornhill, K. L., Winstead, E. L., Cubison, M. J., Hecobian, A., Jimenez, J. L., Weber, R. J., Anderson, B. E., and Nenes, A.: Analysis of CCN activity of Arctic aerosol and Canadian biomass burning during summer 2008, Atmospheric Chem. Phys., 13, 2735–2756, https://doi.org/10.5194/acp-13-2735-2013, 2013.

Lawler, M. J., Lewis, S. L., Russell, L. M., Quinn, P. K., Bates, T. S., Coffman, D. J., Upchurch, L. M., and Saltzman, E. S.: North Atlantic marine organic aerosol characterized by novel offline thermal desorption mass spectrometry: polysaccharides, recalcitrant material, and secondary organics, Atmospheric Chem. Phys., 20, 16007–16022, https://doi.org/10.5194/acp-20-16007-2020, 2020.

Lawrence, C. R. and Neff, J. C.: The contemporary physical and chemical flux of aeolian dust: A synthesis of direct measurements of dust deposition, Chem. Geol., 267, 46–63, https://doi.org/10.1016/j.chemgeo.2009.02.005, 2009.

Levin, E. J. T., McMeeking, G. R., Carrico, C. M., Mack, L. E., Kreidenweis, S. M., Wold, C. E., Moosmüller, H., Arnott, W. P., Hao, W. M., Collett, J. L., and Malm, W. C.: Biomass burning smoke aerosol properties measured during Fire Laboratory at Missoula Experiments (FLAME), J. Geophys. Res., 115, D18210, https://doi.org/10.1029/2009JD013601, 2010.

Levin, Z.: On the interactions of mineral dust, sea-salt particles, and clouds: A measurement and modeling study from the Mediterranean Israeli Dust Experiment campaign, J. Geophys. Res., 110, D20202, https://doi.org/10.1029/2005JD005810, 2005.

Liu, J., Li, Z., and Cribb, M.: Response of Marine Boundary Layer Cloud Properties to Aerosol Perturbations Associated with Meteorological Conditions from the 19-Month AMF-Azores Campaign, J. Atmospheric Sci., 73, 4253–4268, https://doi.org/10.1175/JAS-D-15-0364.1, 2016.

Logan, T., Xi, B., and Dong, X.: Aerosol properties and their influences on marine boundary layer cloud condensation nuclei at the ARM mobile facility over the Azores: Aerosol and influences on MBL CCN, J. Geophys. Res. Atmospheres, 119, 4859–4872, https://doi.org/10.1002/2013JD021288, 2014.

Lopez-Yglesias, X. F., Yeung, M. C., Dey, S. E., Brechtel, F. J., and Chan, C. K.: Performance Evaluation of the Brechtel Mfg. Humidified Tandem Differential Mobility Analyzer (BMI HTDMA) for Studying Hygroscopic Properties of Aerosol Particles, Aerosol Sci. Technol., 48, 969–980, https://doi.org/10.1080/02786826.2014.952366, 2014.

Mahowald, N., Albani, S., Kok, J. F., Engelstaeder, S., Scanza, R., Ward, D. S., and Flanner, M. G.: The size distribution of desert dust aerosols and its impact on the Earth system, Aeolian Res., 15, 53–71, https://doi.org/10.1016/j.aeolia.2013.09.002, 2014a.

Mahowald, N., Albani, S., Kok, J. F., Engelstaeder, S., Scanza, R., Ward, D. S., and Flanner, M. G.: The size distribution of desert dust aerosols and its impact on the Earth system, Aeolian Res., 15, 53–71, https://doi.org/10.1016/j.aeolia.2013.09.002, 2014b.

Maring, H.: Mineral dust aerosol size distribution change during atmospheric transport, J. Geophys. Res., 108, 8592, https://doi.org/10.1029/2002JD002536, 2003.

Massling, A., Nielsen, I. E., Kristensen, D., Christensen, J. H., Sørensen, L. L., Jensen, B., Nguyen, Q. T., Nøjgaard, J. K., Glasius, M., and Skov, H.: Atmospheric black carbon and sulfate concentrations in Northeast Greenland, Atmospheric Chem. Phys., 15, 9681–9692, https://doi.org/10.5194/acp-15-9681-2015, 2015.

Mather, J. H. and Voyles, J. W.: The Arm Climate Research Facility: A Review of Structure and Capabilities, Bull. Am. Meteorol. Soc., 94, 377–392, https://doi.org/10.1175/BAMS-D-11-00218.1, 2013.

Moore, R. H., Karydis, V. A., Capps, S. L., Lathem, T. L., and Nenes, A.: Droplet number uncertainties associated with CCN: an assessment using observations and a global model adjoint, Atmospheric Chem. Phys., 13, 4235–4251, https://doi.org/10.5194/acp-13-4235-2013, 2013.

Mungall, E. L., Abbatt, J. P. D., Wentzell, J. J. B., Lee, A. K. Y., Thomas, J. L., Blais, M., Gosselin, M., Miller, L. A., Papakyriakou, T., Willis, M. D., and Liggio, J.: Microlayer source of oxygenated volatile organic compounds in the summertime marine Arctic boundary layer, Proc. Natl. Acad. Sci., 114, 6203–6208, https://doi.org/10.1073/pnas.1620571114, 2017.

Nakamae, K. and Shiotani, M.: Interannual variability in Saharan dust over the North Atlantic Ocean and its relation to meteorological fields during northern winter, Atmospheric Res., 122, 336–346, https://doi.org/10.1016/j.atmosres.2012.09.012, 2013a.

Ng, N. L., Canagaratna, M. R., Zhang, Q., Jimenez, J. L., Tian, J., Ulbrich, I. M., Kroll, J. H., Docherty, K. S., Chhabra, P. S., Bahreini, R., Murphy, S. M., Seinfeld, J. H., Hildebrandt, L., Donahue, N. M., DeCarlo, P. F., Lanz, V. A., Prévôt, A. S. H., Dinar, E., Rudich, Y., and Worsnop, D. R.: Organic aerosol components observed in Northern Hemispheric datasets from Aerosol Mass Spectrometry, Atmospheric Chem. Phys., 10, 4625–4641, https://doi.org/10.5194/acp-10-4625-2010, 2010.

Ng, N. L., Herndon, S. C., Trimborn, A., Canagaratna, M. R., Croteau, P. L., Onasch, T. B., Sueper, D., Worsnop, D. R., Zhang, Q., Sun, Y. L., and Jayne, J. T.: An Aerosol Chemical Speciation Monitor (ACSM) for Routine Monitoring of the Composition and Mass Concentrations of Ambient Aerosol, Aerosol Sci. Technol., 45, 780–794, https://doi.org/10.1080/02786826.2011.560211, 2011.

O'Dowd, C., Ceburnis, D., Ovadnevaite, J., Vaishya, A., Rinaldi, M., and Facchini, M. C.: Do anthropogenic, continental or coastal aerosol sources impact on a marine aerosol signature at Mace Head?, Atmospheric Chem. Phys., 14, 10687–10704, https://doi.org/10.5194/acp-14-10687-2014, 2014.

O'Dowd, C. D., Smith, M. H., Consterdine, I. E., and Lowe, J. A.: Marine aerosol, sea-salt, and the marine sulphur cycle: a short review, Atmos. Environ., 31, 73–80, https://doi.org/10.1016/S1352-2310(96)00106-9, 1997.

O'Dowd, C. D., Facchini, M. C., Cavalli, F., Ceburnis, D., Mircea, M., Decesari, S., Fuzzi, S., Yoon, Y. J., and Putaud, J.-P.: Biogenically driven organic contribution to marine aerosol, Nature, 431, 676–680, https://doi.org/10.1038/nature02959, 2004.

Omar, A. H., Winker, D. M., Vaughan, M. A., Hu, Y., Trepte, C. R., Ferrare, R. A., Lee, K.-P., Hostetler, C. A., Kittaka, C., Rogers, R. R., Kuehn, R. E., and Liu, Z.: The CALIPSO Automated Aerosol Classification and Lidar Ratio Selection Algorithm, J. Atmospheric Ocean. Technol., 26, 1994–2014, https://doi.org/10.1175/2009JTECHA1231.1, 2009.

Owen, R. C., Cooper, O. R., Stohl, A., and Honrath, R. E.: An analysis of the mechanisms of North American pollutant transport to the central North Atlantic lower free troposphere: LOWER FREE TROPOSPHERE EXPORT MECHANISMS, J. Geophys. Res. Atmospheres, 111, https://doi.org/10.1029/2006JD007062, 2006.

Pandis, S. N., Russell, L. M., and Seinfeld, J. H.: The relationship between DMS flux and CCN concentration in remote marine regions, J. Geophys. Res., 99, 16945, https://doi.org/10.1029/94JD01119, 1994.

Pennypacker, S. and Wood, R.: A Case Study in Low Aerosol Number Concentrations Over the Eastern North Atlantic: Implications for Pristine Conditions in the Remote Marine Boundary Layer, J. Geophys. Res. Atmospheres, 122, 12,393-12,415, https://doi.org/10.1002/2017JD027493, 2017.

Peshev, Z. Y., Deleva, A. D., and Dreischuh, T. N.: Saharan dust mixed with marine aerosols: lidar measurements and characterization, in: 20th International Conference and School on Quantum Electronics: Laser Physics and Applications, 20th

International Conference and School on Quantum Electronics Laser Physics and Applications, Nessebar, Bulgaria, 26, https://doi.org/10.1117/12.2516543, 2019.

Peterson, D. A., Campbell, J. R., Hyer, E. J., Fromm, M. D., Kablick, G. P., Cossuth, J. H., and DeLand, M. T.: Wildfire-driven thunderstorms cause a volcano-like stratospheric injection of smoke, Npj Clim. Atmospheric Sci., 1, 30, https://doi.org/10.1038/s41612-018-0039-3, 2018.

Petters, M. D. and Kreidenweis, S. M.: A single parameter representation of hygroscopic growth and cloud condensation nucleus activity, Atmospheric Chem. Phys., 7, 1961–1971, https://doi.org/10.5194/acp-7-1961-2007, 2007.

Petters, M. D., Carrico, C. M., Kreidenweis, S. M., Prenni, A. J., DeMott, P. J., Collett, J. L., and Moosmüller, H.: Cloud condensation nucleation activity of biomass burning aerosol, J. Geophys. Res., 114, D22205, https://doi.org/10.1029/2009JD012353, 2009.

Pohl, K., Cantwell, M., Herckes, P., and Lohmann, R.: Black carbon concentrations and sources in the marine boundary layer of the tropical Atlantic Ocean using four methodologies, Atmospheric Chem. Phys., 14, 7431–7443, https://doi.org/10.5194/acp-14-7431-2014, 2014.

Quinn, P. K. and Bates, T. S.: The case against climate regulation via oceanic phytoplankton sulphur emissions, Nature, 480, 51–56, https://doi.org/10.1038/nature10580, 2011.

Quinn, P. K., Bates, T. S., Coffman, D. J., Upchurch, L., Johnson, J. E., Moore, R., Ziemba, L., Bell, T. G., Saltzman, E. S., Graff, J., and Behrenfeld, M. J.: Seasonal Variations in Western North Atlantic Remote Marine Aerosol Properties, J. Geophys. Res. Atmospheres, 124, 14240–14261, https://doi.org/10.1029/2019JD031740, 2019.

Redemann, J., Wood, R., Zuidema, P., Doherty, S. J., Luna, B., LeBlanc, S. E., Diamond, M. S., Shinozuka, Y., Chang, I. Y., Ueyama, R., Pfister, L., Ryoo, J.-M., Dobracki, A. N., da Silva, A. M., Longo, K. M., Kacenelenbogen, M. S., Flynn, C. J., Pistone, K., Knox, N. M., Piketh, S. J., Haywood, J. M., Formenti, P., Mallet, M., Stier, P., Ackerman, A. S., Bauer, S. E., Fridlind, A. M., Carmichael, G. R., Saide, P. E., Ferrada, G. A., Howell, S. G., Freitag, S., Cairns, B., Holben, B. N., Knobelspiesse, K. D., Tanelli, S., L'Ecuyer, T. S., Dzambo, A. M., Sy, O. O., McFarquhar, G. M., Poellot, M. R., Gupta, S., O'Brien, J. R., Nenes, A., Kacarab, M., Wong, J. P. S., Small-Griswold, J. D., Thornhill, K. L., Noone, D., Podolske, J. R., Schmidt, K. S., Pilewskie, P., Chen, H., Cochrane, S. P., Sedlacek, A. J., Lang, T. J., Stith, E., Segal-Rozenhaimer, M., Ferrare, R. A., Burton, S. P., Hostetler, C. A., Diner, D. J., Seidel, F. C., Platnick, S. E., Myers, J. S., Meyer, K. G., Spangenberg, D. A., Maring, H., and Gao, L.: An overview of the ORACLES (ObseRvations of Aerosols above CLouds and their intEractionS) project: aerosol–cloud–radiation interactions in the southeast Atlantic basin, Atmospheric Chem. Phys., 21, 1507–1563, https://doi.org/10.5194/acp-21-1507-2021, 2021.

Rémillard, J. and Tselioudis, G.: Cloud Regime Variability over the Azores and Its Application to Climate Model Evaluation, J. Clim., 28, 9707–9720, https://doi.org/10.1175/JCLI-D-15-0066.1, 2015.

Rémillard, J., Kollias, P., Luke, E., and Wood, R.: Marine Boundary Layer Cloud Observations in the Azores, J. Clim., 25, 7381–7398, https://doi.org/10.1175/JCLI-D-11-00610.1, 2012.

Riemer, N., Doherty, O. M., and Hameed, S.: On the variability of African dust transport across the Atlantic, Geophys. Res. Lett., 33, L13814, https://doi.org/10.1029/2006GL026163, 2006.

Rinaldi, M., Decesari, S., Finessi, E., Giulianelli, L., Carbone, C., Fuzzi, S., O'Dowd, C. D., Ceburnis, D., and Facchini, M. C.: Primary and Secondary Organic Marine Aerosol and Oceanic Biological Activity: Recent Results and New Perspectives for Future Studies, Adv. Meteorol., 2010, 1–10, https://doi.org/10.1155/2010/310682, 2010.

Roberts, G., Mauger, G., Hadley, O., and Ramanathan, V.: North American and Asian aerosols over the eastern Pacific Ocean and their role in regulating cloud condensation nuclei, J. Geophys. Res., 111, D13205, https://doi.org/10.1029/2005JD006661, 2006.

Roberts, G. C. and Nenes, A.: A Continuous-Flow Streamwise Thermal-Gradient CCN Chamber for Atmospheric Measurements, Aerosol Sci. Technol., 39, 206–221, https://doi.org/10.1080/027868290913988, 2005.

Rose, D., Gunthe, S. S., Mikhailov, E., Frank, G. P., Dusek, U., Andreae, M. O., and Pöschl, U.: Calibration and measurement uncertainties of a continuous-flow cloud condensation nuclei counter (DMT-CCNC): CCN activation of ammonium sulfate and sodium chloride aerosol particles in theory and experiment, Atmospheric Chem. Phys., 8, 1153–1179, https://doi.org/10.5194/acp-8-1153-2008, 2008.

Rosenfeld, D., Andreae, M. O., Asmi, A., Chin, M., de Leeuw, G., Donovan, D. P., Kahn, R., Kinne, S., Kivekäs, N., Kulmala, M., Lau, W., Schmidt, K. S., Suni, T., Wagner, T., Wild, M., and Quaas, J.: Global observations of aerosol-cloud-precipitation-

climate interactions: Aerosol-cloud-climate interactions, Rev. Geophys., 52, 750–808, https://doi.org/10.1002/2013RG000441, 2014.

Sakerin, S. M., Kabanov, D. M., Kopeikin, V. M., Kruglinsky, I. A., Novigatsky, A. N., Pol'kin, V. V., Shevchenko, V. P., and Turchinovich, Y. S.: Spatial Distribution of Black Carbon Concentrations in the Atmosphere of the North Atlantic and the European Sector of the Arctic Ocean, Atmosphere, 12, 949, https://doi.org/10.3390/atmos12080949, 2021.

Saliba, G., Chen, C., Lewis, S., Russell, L. M., Quinn, P. K., Bates, T. S., Bell, T. G., Lawler, M. J., Saltzman, E. S., Sanchez, K. J., Moore, R., Shook, M., Rivellini, L., Lee, A., Baetge, N., Carlson, C. A., and Behrenfeld, M. J.: Seasonal Differences and Variability of Concentrations, Chemical Composition, and Cloud Condensation Nuclei of Marine Aerosol Over the North Atlantic, J. Geophys. Res. Atmospheres, 125, https://doi.org/10.1029/2020JD033145, 2020.

Sanchez, K. J., Chen, C.-L., Russell, L. M., Betha, R., Liu, J., Price, D. J., Massoli, P., Ziemba, L. D., Crosbie, E. C., Moore, R. H., Müller, M., Schiller, S. A., Wisthaler, A., Lee, A. K. Y., Quinn, P. K., Bates, T. S., Porter, J., Bell, T. G., Saltzman, E. S., Vaillancourt, R. D., and Behrenfeld, M. J.: Substantial Seasonal Contribution of Observed Biogenic Sulfate Particles to Cloud Condensation Nuclei, Sci. Rep., 8, 3235, https://doi.org/10.1038/s41598-018-21590-9, 2018.

Sanchez, K. J., Zhang, B., Liu, H., Brown, M. D., Crosbie, E. C., Gallo, F., Hair, J. W., Hostetler, C. A., Jordan, C. E., Robinson, C. E., Scarino, A. J., Shingler, T. J., Shook, M. A., Thornhill, K. L., Wiggins, E. B., Winstead, E. L., Ziemba, L. D., Saliba, G., Lewis, S. L., Russell, L. M., Quinn, P. K., Bates, T. S., Porter, J., Bell, T. G., Gaube, P., Saltzman, E. S., Behrenfeld, M. J., and Moore, R. H.: North Atlantic Ocean SST-gradient-driven variations in aerosol and cloud evolution along Lagrangian cold-air outbreak trajectories, Atmospheric Chem. Phys., 22, 2795–2815, https://doi.org/10.5194/acp-22-2795-2022, 2022.

Seinfeld, J. H., Bretherton, C., Carslaw, K. S., Coe, H., DeMott, P. J., Dunlea, E. J., Feingold, G., Ghan, S., Guenther, A. B., Kahn, R., Kraucunas, I., Kreidenweis, S. M., Molina, M. J., Nenes, A., Penner, J. E., Prather, K. A., Ramanathan, V., Ramaswamy, V., Rasch, P. J., Ravishankara, A. R., Rosenfeld, D., Stephens, G., and Wood, R.: Improving our fundamental understanding of the role of aerosol−cloud interactions in the climate system, Proc. Natl. Acad. Sci., 113, 5781–5790, https://doi.org/10.1073/pnas.1514043113, 2016.

Shank, L. M., Howell, S., Clarke, A. D., Freitag, S., Brekhovskikh, V., Kapustin, V., McNaughton, C., Campos, T., and Wood, R.: Organic matter and non-refractory aerosol over the remote Southeast Pacific: oceanic and combustion sources, Atmospheric Chem. Phys., 12, 557–576, https://doi.org/10.5194/acp-12-557-2012, 2012.

Sharon, T. M., Albrecht, B. A., Jonsson, H. H., Minnis, P., Khaiyer, M. M., van Reken, T. M., Seinfeld, J., and Flagan, R.: Aerosol and Cloud Microphysical Characteristics of Rifts and Gradients in Maritime Stratocumulus Clouds, J. Atmospheric Sci., 63, 983–997, https://doi.org/10.1175/JAS3667.1, 2006.

Sorooshian, A., Corral, A. F., Braun, R. A., Cairns, B., Crosbie, E., Ferrare, R., Hair, J., Kleb, M. M., Hossein Mardi, A., Maring, H., McComiskey, A., Moore, R., Painemal, D., Scarino, A. J., Schlosser, J., Shingler, T., Shook, M., Wang, H., Zeng, X., Ziemba, L., and Zuidema, P.: Atmospheric Research Over the Western North Atlantic Ocean Region and North American East Coast: A Review of Past Work and Challenges Ahead, J. Geophys. Res. Atmospheres, 125, https://doi.org/10.1029/2019JD031626, 2020.

Springston, S.: Particle Soot Absorption Photometer (PSAP) Instrument Handbook, https://doi.org/10.2172/1246162, 2018.

Stein, A. F., Draxler, R. R., Rolph, G. D., Stunder, B. J. B., Cohen, M. D., and Ngan, F.: NOAA's HYSPLIT Atmospheric Transport and Dispersion Modeling System, Bull. Am. Meteorol. Soc., 96, 2059–2077, https://doi.org/10.1175/BAMS-D-14-00110.1, 2015.

Swietlicki, E., Hansson, H.-C., Hämeri, K., Svenningsson, B., Massling, A., McFiggans, G., McMurry, P. H., Petäjä, T., Tunved, P., Gysel, M., Topping, D., Weingartner, E., Baltensperger, U., Rissler, J., Wiedensohler, A., and Kulmala, M.: Hygroscopic properties of submicrometer atmospheric aerosol particles measured with H-TDMA instruments in various environments—a review, Tellus B Chem. Phys. Meteorol., 60, 432, https://doi.org/10.1111/j.1600-0889.2008.00350.x, 2008.

Thunis, P., Degraeuwe, B., Pisoni, E., Trombetti, M., Peduzzi, E., Belis, C. A., Wilson, J., Clappier, A., and Vignati, E.: PM2.5 source allocation in European cities: A SHERPA modelling study, Atmos. Environ., 187, 93–106, https://doi.org/10.1016/j.atmosenv.2018.05.062, 2018.

Tobo, Y., Adachi, K., DeMott, P. J., Hill, T. C. J., Hamilton, D. S., Mahowald, N. M., Nagatsuka, N., Ohata, S., Uetake, J., Kondo, Y., and Koike, M.: Glacially sourced dust as a potentially significant source of ice nucleating particles, Nat. Geosci., 12, 253–258, https://doi.org/10.1038/s41561-019-0314-x, 2019.

Tomlin, J. M., Jankowski, K. A., Veghte, D. P., China, S., Wang, P., Fraund, M., Weis, J., Zheng, G., Wang, Y., Rivera-Adorno, F., Raveh-Rubin, S., Knopf, D. A., Wang, J., Gilles, M. K., Moffet, R. C., and Laskin, A.: Impact of dry intrusion events on the composition and mixing state of particles during the winter Aerosol and Cloud Experiment in the Eastern North Atlantic (ACE-ENA), Atmospheric Chem. Phys., 21, 18123–18146, https://doi.org/10.5194/acp-21-18123-2021, 2021.

5 Twomey, S.: Pollution and the planetary albedo, Atmospheric Environ. 1967, 8, 1251–1256, https://doi.org/10.1016/0004-6981(74)90004-3, 1974.

Uin, J.: Ultra-High-Sensitivity Aerosol Spectrometer (UHSAS) Instrument Handbook, https://doi.org/10.2172/1251410, 2016a.

Uin, J.: Cloud Condensation Nuclei Counter (CCN) Instrument Handbook, 2016b.

10 Uin, J.: 3002 Humidified Tandem Differential Mobility Analyzer Instrument Handbook, 2016c.

Uin, J.: Integrating Nephelometer Instrument Handbook, https://doi.org/10.2172/1246075, 2016d.

Uin, J. and Smith, S.: Eastern North Atlantic (ENA) Aerosol Observing System (AOS) Instrument Handbook, 2020.

Uin, J., Aiken, A. C., Dubey, M. K., Kuang, C., Pekour, M., Salwen, C., Sedlacek, A. J., Senum, G., Smith, S., Wang, J., Watson, T. B., and Springston, S. R.: Atmospheric Radiation Measurement (ARM) Aerosol Observing Systems (AOS) for
15 Surface-Based In Situ Atmospheric Aerosol and Trace Gas Measurements, J. Atmospheric Ocean. Technol., 36, 2429–2447, https://doi.org/10.1175/JTECH-D-19-0077.1, 2019.

Vignati, E., Facchini, M. C., Rinaldi, M., Scannell, C., Ceburnis, D., Sciare, J., Kanakidou, M., Myriokefalitakis, S., Dentener, F., and O'Dowd, C. D.: Global scale emission and distribution of sea-spray aerosol: Sea-salt and organic enrichment, Atmos. Environ., 44, 670–677, https://doi.org/10.1016/j.atmosenv.2009.11.013, 2010.

20 Virkkula, A.: Correction of the Calibration of the 3-wavelength Particle Soot Absorption Photometer (3λ PSAP), Aerosol Sci. Technol., 44, 706–712, https://doi.org/10.1080/02786826.2010.482110, 2010.

Virkkula, A., Ahlquist, N. C., Covert, D. S., Arnott, W. P., Sheridan, P. J., Quinn, P. K., and Coffman, D. J.: Modification, Calibration and a Field Test of an Instrument for Measuring Light Absorption by Particles, Aerosol Sci. Technol., 39, 68–83, https://doi.org/10.1080/027868290901963, 2005.

25 Wang, J., Wood, R., Jensen, M. P., Chiu, J. C., Liu, Y., Lamer, K., Desai, N., Giangrande, S. E., Knopf, D. A., Kollias, P., Laskin, A., Liu, X., Lu, C., Mechem, D., Mei, F., Starzec, M., Tomlinson, J., Wang, Y., Yum, S. S., Zheng, G., Aiken, A. C., Azevedo, E. B., Blanchard, Y., China, S., Dong, X., Gallo, F., Gao, S., Ghate, V. P., Glienke, S., Goldberger, L., Hardin, J. C., Kuang, C., Luke, E. P., Matthews, A. A., Miller, M. A., Moffet, R., Pekour, M., Schmid, B., Sedlacek, A. J., Shaw, R. A., Shilling, J. E., Sullivan, A., Suski, K., Veghte, D. P., Weber, R., Wyant, M., Yeom, J., Zawadowicz, M., and Zhang, Z.: Aerosol
30 and Cloud Experiments in the Eastern North Atlantic (ACE-ENA), Bull. Am. Meteorol. Soc., 1–51, https://doi.org/10.1175/BAMS-D-19-0220.1, 2021a.

Wang, Y., Zheng, G., Jensen, M., Knopf, D., Laskin, A., Matthews, A., Mechem, D., Mei, F., Moffet, R., Sedlacek, A., Shilling, J., Springston, S., Sullivan, A., Tomlinson, J., Veghte, D., Weber, R., Wood, R., Zawadowicz, M., and Wang, J.: Vertical profiles of trace gas and aerosol properties over the Eastern North Atlantic: Variations with season and synoptic condition,
35 Aerosols/Field Measurements/Troposphere/Physics (physical properties and processes), https://doi.org/10.5194/acp-2021-300, 2021b.

Watson, T. B.: Aerosol Chemical Speciation Monitor (ACSM) Instrument Handbook, https://doi.org/10.2172/1375336, 2017.

Wood, R.: Stratocumulus Clouds, Mon. Weather Rev., 140, 2373–2423, https://doi.org/10.1175/MWR-D-11-00121.1, 2012.

Wood, R., Wyant, M., Bretherton, C. S., Rémillard, J., Kollias, P., Fletcher, J., Stemmler, J., Szoeke, S. de, Yuter, S., Miller,
40 M., Mechem, D., Tselioudis, G., Chiu, J. C., Mann, J. A. L., O'Connor, E. J., Hogan, R. J., Dong, X., Miller, M., Ghate, V., Jefferson, A., Min, Q., Minnis, P., Palikonda, R., Albrecht, B., Luke, E., Hannay, C., and Lin, Y.: Clouds, Aerosols, and Precipitation in the Marine Boundary Layer: An Arm Mobile Facility Deployment, Bull. Am. Meteorol. Soc., 96, 419–440, https://doi.org/10.1175/BAMS-D-13-00180.1, 2015.

Wood, R., Stemmler, J. D., Rémillard, J., and Jefferson, A.: Low-CCN concentration air masses over the eastern North Atlantic:
45 Seasonality, meteorology, and drivers, J. Geophys. Res. Atmospheres, 122, 1203–1223, https://doi.org/10.1002/2016JD025557, 2017.

Wu, P., Dong, X., Xi, B., Tian, J., and Ward, D. M.: Profiles of MBL Cloud and Drizzle Microphysical Properties Retrieved From Ground-Based Observations and Validated by Aircraft In Situ Measurements Over the Azores, J. Geophys. Res. Atmospheres, 125, https://doi.org/10.1029/2019JD032205, 2020.

Yang, Y., Lou, S., Wang, H., Wang, P., and Liao, H.: Trends and source apportionment of aerosols in Europe during 1980–2018, Atmospheric Chem. Phys., 20, 2579–2590, https://doi.org/10.5194/acp-20-2579-2020, 2020.

Yeom, J. M., Yum, S. S., Shaw, R. A., La, I., Wang, J., Lu, C., Liu, Y., Mei, F., Schmid, B., and Matthews, A.: Vertical Variations of Cloud Microphysical Relationships in Marine Stratocumulus Clouds Observed During the ACE-ENA Campaign, J. Geophys. Res. Atmospheres, 126, https://doi.org/10.1029/2021JD034700, 2021.

Yoon, Y. J., Ceburnis, D., Cavalli, F., Jourdan, O., Putaud, J. P., Facchini, M. C., Decesari, S., Fuzzi, S., Sellegri, K., Jennings, S. G., and O'Dowd, C. D.: Seasonal characteristics of the physicochemical properties of North Atlantic marine atmospheric aerosols, J. Geophys. Res., 112, D04206, https://doi.org/10.1029/2005JD007044, 2007.

Zawadowicz, M. A., Suski, K., Liu, J., Pekour, M., Fast, J., Mei, F., Sedlacek, A., Springston, S., Wang, Y., Zaveri, R. A., Wood, R., Wang, J., and Shilling, J. E.: Aircraft measurements of aerosol and trace gas chemistry in theEastern North Atlantic, Aerosols/Field Measurements/Troposphere/Chemistry (chemical composition and reactions), https://doi.org/10.5194/acp-2020-887, 2020.

Zellner, R.: [No title found], J. Atmospheric Chem., 37, 212–214, https://doi.org/10.1023/A:1006483708571, 2000.

Zhang, B., Owen, R. C., Perlinger, J. A., Helmig, D., Val Martín, M., Kramer, L., Mazzoleni, L. R., and Mazzoleni, C.: Ten-year chemical signatures associated with long-range transport observed in the free troposphere over the central North Atlantic, Elem. Sci. Anthr., 5, 8, https://doi.org/10.1525/elementa.194, 2017.

Zhang, X., Massoli, P., Quinn, P. K., Bates, T. S., and Cappa, C. D.: Hygroscopic growth of submicron and supermicron aerosols in the marine boundary layer, J. Geophys. Res. Atmospheres, 119, 8384–8399, https://doi.org/10.1002/2013JD021213, 2014.

Zhao, T. L., Gong, S. L., Huang, P., and Lavoué, D.: Hemispheric transport and influence of meteorology on global aerosol climatology, Atmospheric Chem. Phys., 12, 7609–7624, https://doi.org/10.5194/acp-12-7609-2012, 2012.

Zheng, G., Wang, Y., Aiken, A. C., Gallo, F., Jensen, M. P., Kollias, P., Kuang, C., Luke, E., Springston, S., Uin, J., Wood, R., and Wang, J.: Marine boundary layer aerosol in the eastern North Atlantic: seasonal variations and key controlling processes, Atmospheric Chem. Phys., 18, 17615–17635, https://doi.org/10.5194/acp-18-17615-2018, 2018.

Zheng, G., Sedlacek, A. J., Aiken, A. C., Feng, Y., Watson, T. B., Raveh-Rubin, S., Uin, J., Lewis, E. R., and Wang, J.: Long-range transported North American wildfire aerosols observed in marine boundary layer of eastern North Atlantic, Environ. Int., 139, 105680, https://doi.org/10.1016/j.envint.2020.105680, 2020.

Zheng, G., Wang, Y., Wood, R., Jensen, M. P., Kuang, C., McCoy, I. L., Matthews, A., Mei, F., Tomlinson, J. M., Shilling, J. E., Zawadowicz, M. A., Crosbie, E., Moore, R., Ziemba, L., Andreae, M. O., and Wang, J.: New particle formation in the remote marine boundary layer, Nat. Commun., 12, 527, https://doi.org/10.1038/s41467-020-20773-1, 2021.

Tables and figures

Table 1. Aerosol Observing System measurements at ENA ARM site analyzed in this study.

Measurement	Symbol	Unit	Instrument	Refrence
Submicron aerosol number concentration	N_{tot}	cm^{-3}	Condensation Particle Counter CPC Model 3772, TSI Inc.	(Kuang et al., 2019)
Size distribution of submicron aerosols (70 to 1000 nm)		cm^{-3}	Ultra-High-Sensitivity Aerosol Spectometer UHSAS, DMT	(Uin et. al, 2016a)
Number concentration of cloud condensation nuclei	CCN	cm^{-3}	Cloud Condensation Nuclei Counter CCN Model CCN-100, DMT	(Roberts and Nenes, 2005; Rose et al., 2008; Uin et. al, 2016b)
Aerosol growth factor			Humidified Tandem Differential Mobility Analyzer HTDMA Model 3002, Bretchel	(Lopez-Yglesias et al., 2014; Uin et. al, 2016c)
Aerosol absorption coefficients	B_{abs}	Mm^{-1}	Particle Soot Absorption Photometer PSAP 3-λ, Radiant Research	(Bond et al., 1999; Virkkula et al., 2005; Virkkula, 2010; Springston, 2018)
Aerosol scattering coefficients	B_{sca}	Mm^{-1}	Integrating Nephelometer Neph, Model 3563, TSI	(Costabile et al., 2013; Uin et. al, 2016d)
Non-refractory sufate and organic		µm^{-3}	Aerosol Chemical Speciation Monitor Aerodyne Research	(Ng et al., 2011; Watson, 2017)

Table 2. Summary of multiday transported aerosol plumes events that affected ENA in 2017 including duration, aerosol emission origins, CALIPSO classification. The values of the three aerosol properties used by the algorithm to detect the events (median concentration of particles with D_p 100-1000 nm, median SSA 1 µm at λ 464 nm, and mean BC values) are shown in the rightmost column during each

10 event (first line) and under baseline condition (in italic, second line).

Event	Duration (hours)	Origin (Hysplit)	CALIPSO aerosol classification	Median concentration particles D_p100-1000 nm	Median SSA 1 µm (λ 464 nm)	Mean BC (ng m^{-3})
January 07 to 11	114	Northern Europe	Mixture of dust, polluted continental aerosols and smoke	365 cm^{-3} *83 cm^{-3}*	0.87 *0.96*	229 ± 41 ng m^{-3} *36 ± 21 ng m^{-3}*
March 12 to 15	72	Arctic/Canada	Mixture of dust, and marine aerosols	319 cm^{-3} *91 cm^{-3}*	0.93 *0.96*	115 ± 37 ng m^{-3} *35 ± 19 ng m^{-3}*
April 20 to 22	54	Northern Europe	Mixture of marine and polluted continental aerosols, and smoke	460 cm^{-3} *99 cm^{-3}*	0.94 *0.95*	121 ± 27 ng m^{-3} *29 ± 21 ng m^{-3}*
May 21 to 22	36	North America	Polluted continental aerosol and smoke	608 cm^{-3} *93 cm^{-3}*	0.94 *0.97*	142 ± 16 ng m^{-3} *33 ± 20 ng m^{-3}*
August 26 to 29	84	North America	Elevated smoke	332 cm^{-3} *105 cm^{-3}*	0.94 *0.95*	181 ± 58 ng m^{-3} *40 ± 25 ng m^{-3}*
September 09 to 13	96	North America/Canada	Data not available	289 cm^{-3} *103 cm^{-3}*	0.93 *0.96*	175 ± 39 ng m^{-3} *39 ± 22 ng m^{-3}*
October 11 to 13	48	Hurricane Ophelia	Mixture of dust, marine and polluted continental aerosols, and smoke	329 cm^{-3} *99 cm^{-3}*	0.89 *0.96*	144 ± 69 ng m^{-3} *30 ± 19 ng m^{-3}*
November 26 to28	54	North Africa	Mixture of dust, and marine aerosols	271 cm^{-3} *81 cm^{-3}*	0.91 *0.96*	181 ± 29 ng m^{-3} *34 ± 21 ng m^{-3}*
December 07 to 10	84	North Africa	Mixture of dust, and marine aerosols	235 cm^{-3} *80 cm^{-3}*	0.92 *0.96*	103 ± 18 ng m^{-3} *26 ± 18 ng m^{-3}*

Table 3. Summary of the characteristics of each type of multiday aerosol plume transport event. Underlined values indicate statistically significant Δ

	Dust and Marine mixture	Polluted continental and Marine mixture	Biomass Burning
Events Date (year 2017) and Origin	• March 12 to 15 – Arctic/Canada • November 26 to28 – North Africa • December 07 to 10 – North Africa	• January 07 to 11 – North Europe • April 20 to 22 – North Europe • May 21 to 22 – North America • October 11 to 13 – Hurricane	• August 26 to 29 – North America • September 09 to 13 – North America
Statistical analysis			
ΔN_{tot}	≥ 110%	Between 95% and 110%	< 25%
$\Delta N_{At}/ N_{Ac}$	< 1%	≥ 200%	≥ 200%
$\Delta AF_{0.1\%}$	~ 5% SS 0.1%	Between 30% and 75%	≥ 75%

$\Delta AF_{0.1\%}$	~ 7% SS 0.2%	Between 35% and 100%	> 75%
Size mode fraction			
N_{At} contribution to N_{tot}	~ 59%	~ 42%	~ 33%
N_{Ac} contribution to N_{tot}	~ 38%	~ 56%	~ 63%
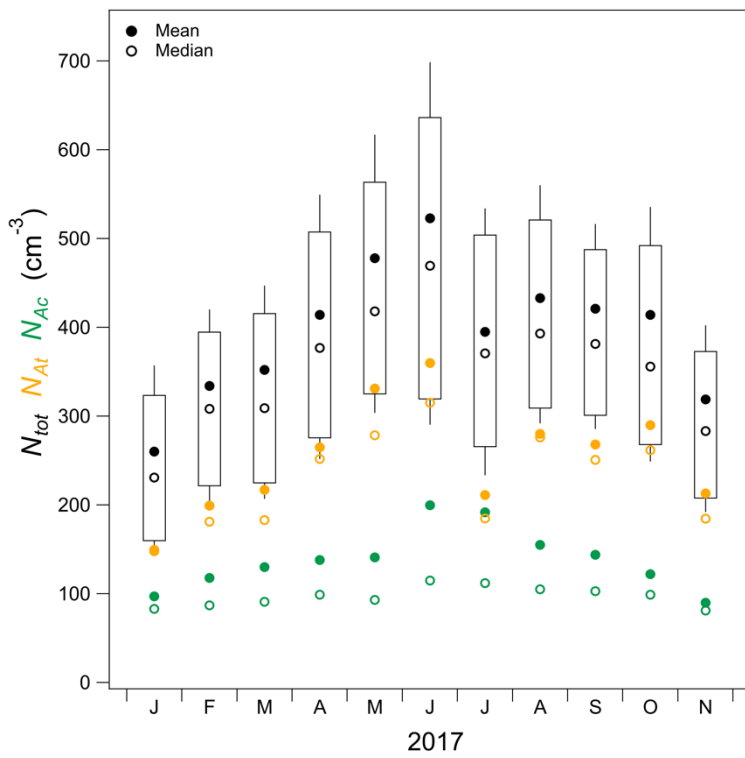
Figure 1. Box and whisker plot of monthly ubmicron aerosol number concentrations (box bottom at 25%, box top at 75%, whisker bottom at 10%, and whisker top at 90%). Mean (circles) and median (open circles) of total number concentration (black), number of Aitken (yellow), and Accumulation (green) modes.
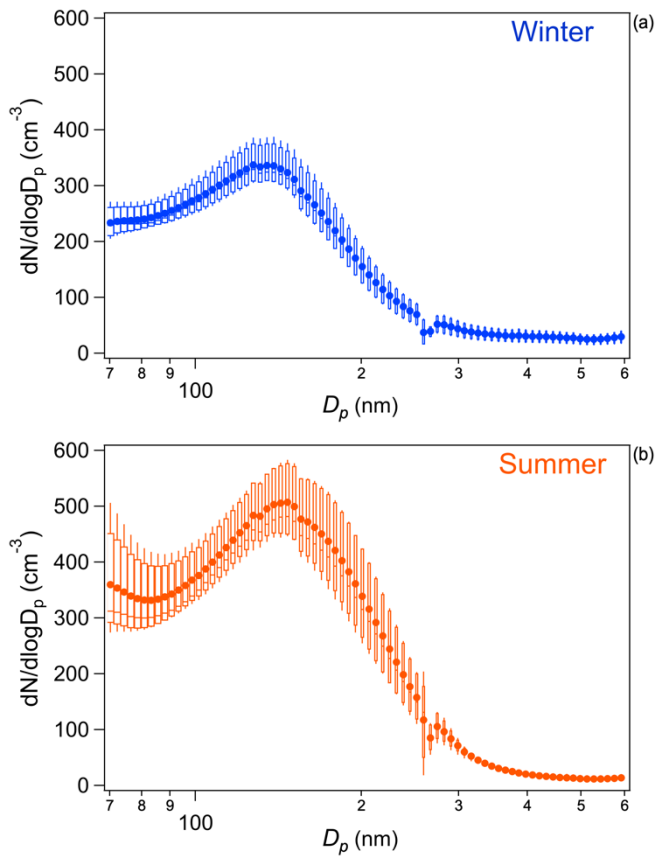
Figure 2. Particle size distribution in winter (a) and summer (b) 2017, per each size bean mean circle, and median -, box bottom at 25%, box top at 75%, whisker bottom at 10%, and whisker top at 90%). Discontinuity at around 270 nm due to technical limitations 10 of the UHSAS (handoff region between two internal gain stages).
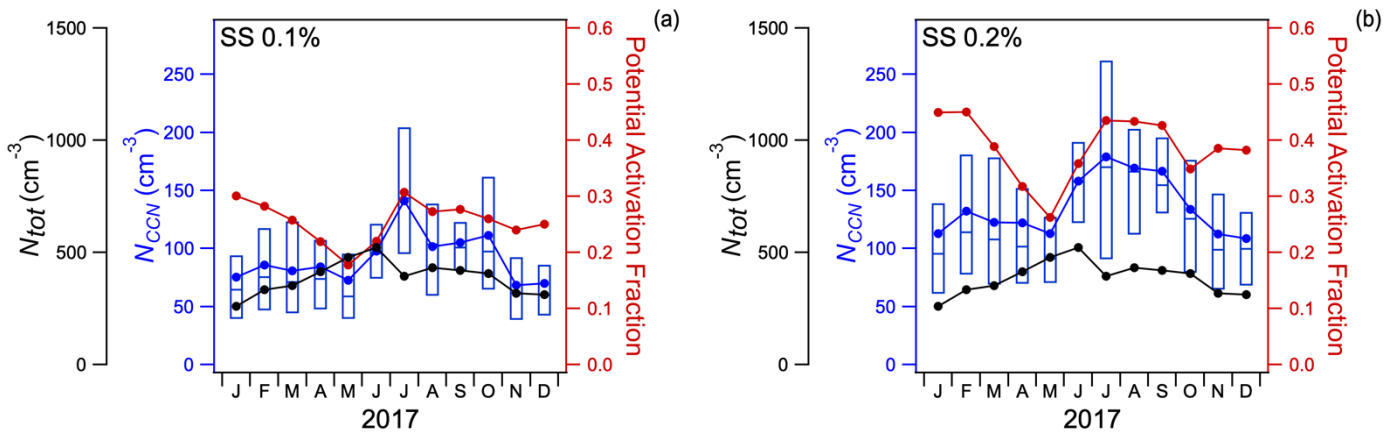
Figure 3. Box and whisker plot of $N_{CCN,0.1\%}$ (a) and $N_{CCN,0.2\%}$ (b), mean N_{CCN} blue circles, median -, box bottom at 25%, box top at 75%, whisker bottom at 10%, and whisker top at 90%, mean N_{tot}, black circles, and CCN potential activation fraction red circles.
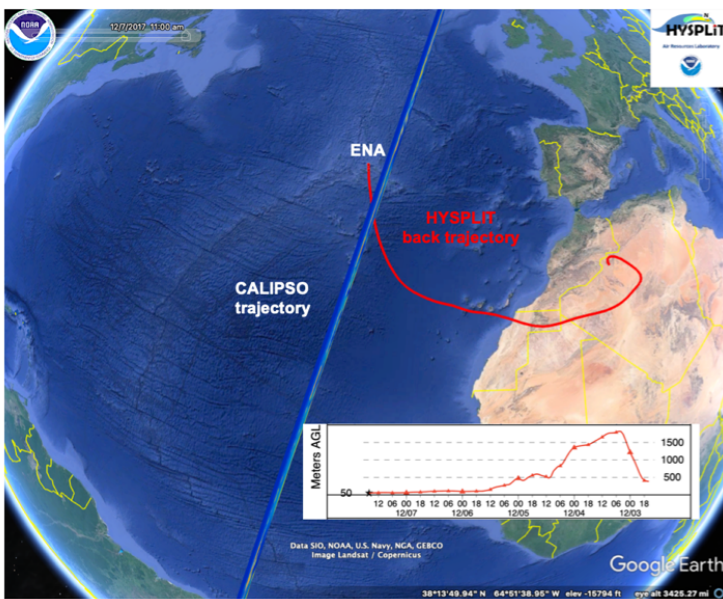
Figure 4. CALIPSO trajectories (blue) and Hysplit back trajectories (red) arriving at 50 m a.g.l. above the ENA site on December 07, 2017 (© Google Earth 2015).
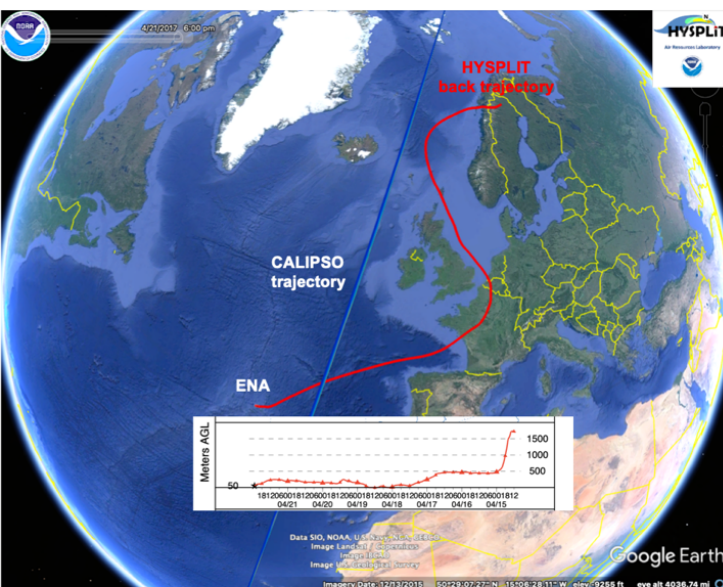
Figure 5. CALIPSO trajectories (blue), and Hysplit back trajectories (red) arriving at 50 m a.g.l. above the ENA site on April 21, 2017 (© Google Earth 2015).
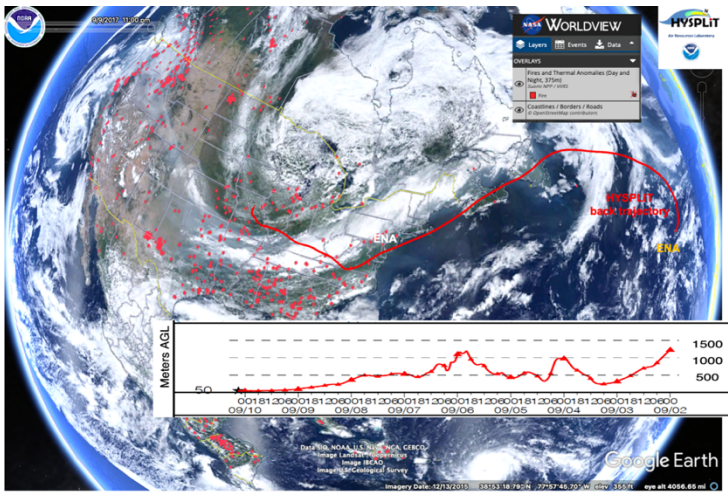
5   **Figure 6.** NASA Worldview VIIRS 375 Active fires between September 1 and 15, 2017 (red circles), and Hysplit back trajectories arriving at 50 m a.g.l. above the ENA site on September 10, 2017 (© Google Earth 2015).
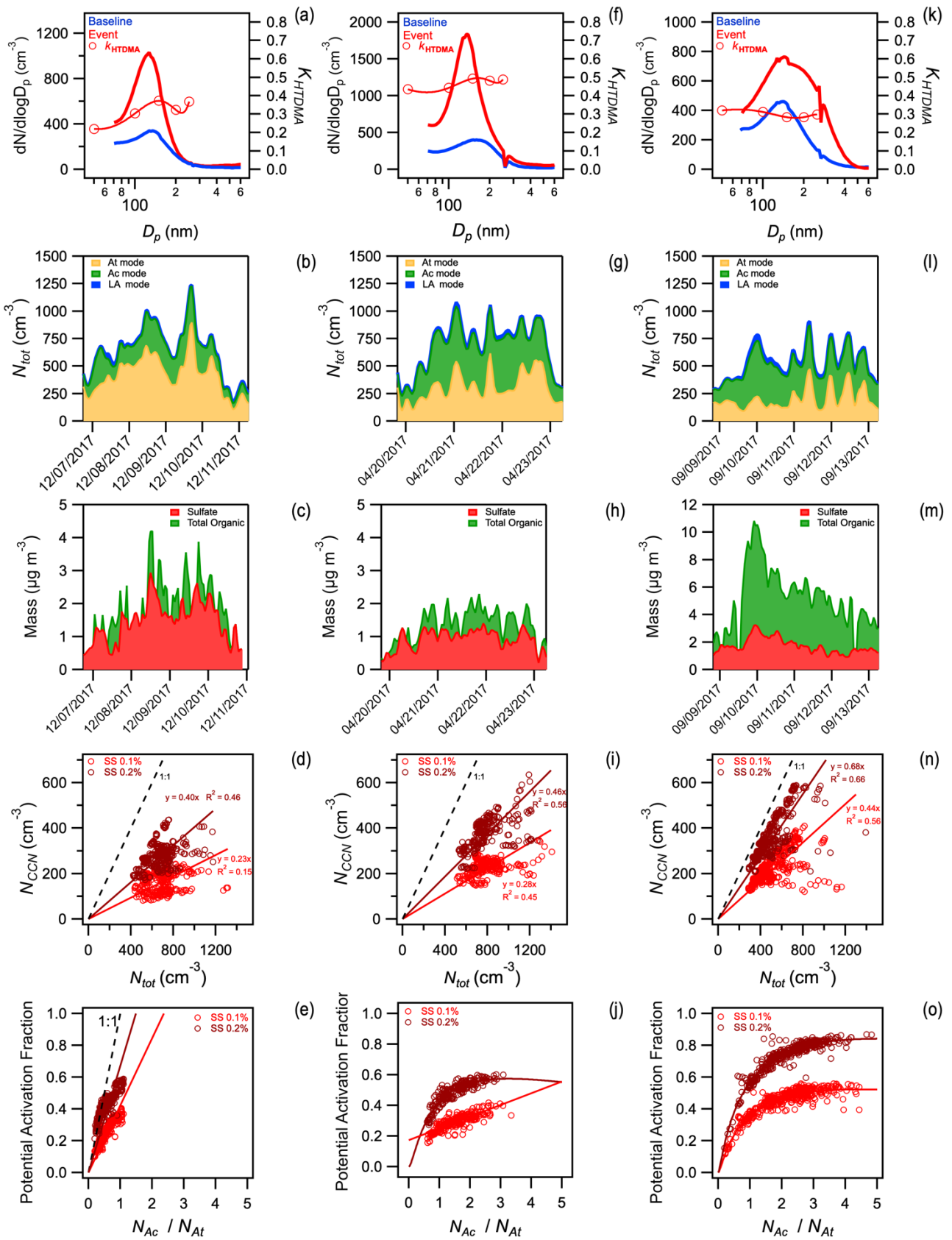
Figure 7. Case study of December 2017 (leftmost), April 2017 (center), and September 2017 (rightmost) events. Submicron particle size distribution under baseline conditions (blue) and during the events (red), and κ_{HTDMA} (open circles) during the events (a, f, k), Aitken, Accumulation, and Large Accumulation mode contributions to (b, g, l), non-refractory sulfate and organic aerosols (c, h, m), scatter plot of N_{CCN} versus N_{tot} during the event (red circle) and fitting lines for the events at SS 0.1% (red) and at SS 0.2% (dark red) (d, i, n), plot of potential activation ratio versus N_{Ac} / N_{At}, or the events at SS 0.1% (red) and at SS 0.2% (dark red) (e, j, o).
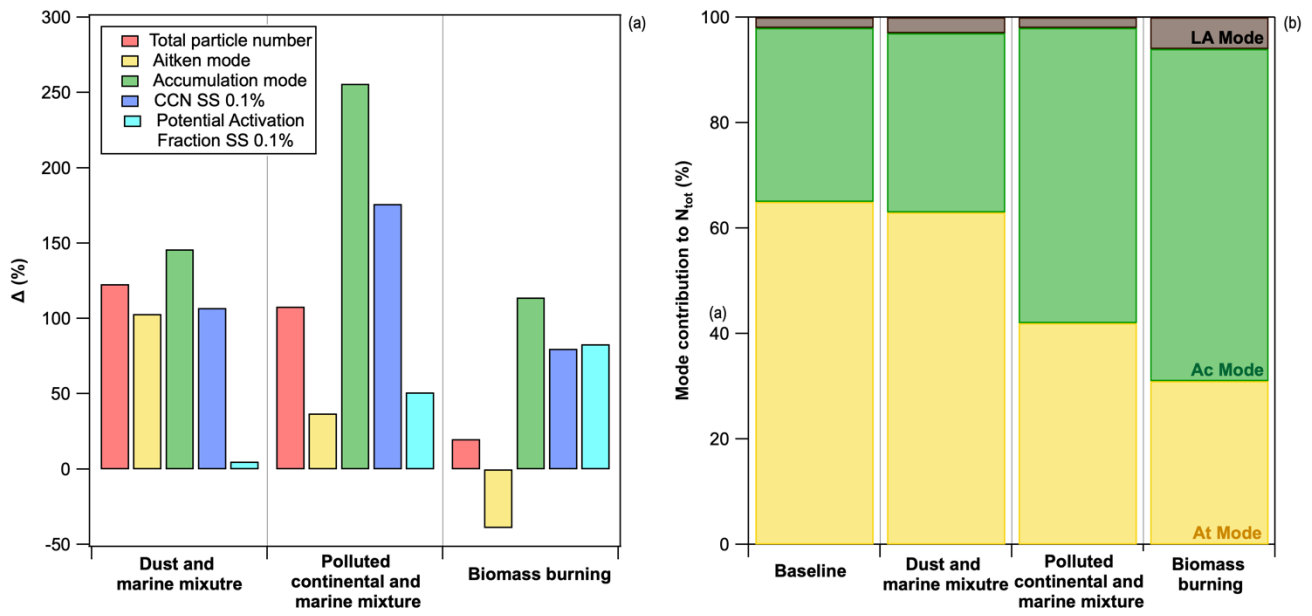
Figure 8. Mean percentage change in N_{tot}, N_{At}, N_{Ac}, $N_{CCN-0.1\%}$, and CCN potential activation fraction at SS 0.1% for each type of event (a); Aitken, Accumulation and Large Accumulation particle modes relative contribution to N_{tot}, for baseline and each type of event.